Title

Lava flow eruption conditions in the Tharsis Volcanic Province on Mars

S. I. Peters[1], P. R. Christensen[1], and A.B. Clarke[1,2]. [1]School of Earth and Space Exploration, Arizona State University, Tempe, AZ 85281, USA. [2] Istituto Nazionale di Geofisica e Vulcanologia, Sezione di Pisa, Pisa, Italy.

Corresponding author: Sean I. Peters, School of Earth and Space Exploration, Arizona State University, Tempe, AZ, 85281, USA. (speter24@asu.edu)

Key Points:

- Terrestrial effusion rates and compositions explain many Martian lava flow morphologies
- Martian lava flows require large and/or long-lived subsurface pathways to transport large volumes to surface
- Differences in eruption rates across Tharsis indicate different source conditions and different conditions in subsurface conduits

Abstract

Volcanism has played a major role in modifying the Martian surface. The Tharsis Volcanic Province dominates the western hemisphere of the planet with numerous effusive volcanic constructs and deposits. Here, we present the results of an in-depth study aimed at characterizing and modelling the emplacement conditions of 40 lava flows in the Tharsis Volcanic Province. These lava flows display a range of lengths (~15 – 314 km), widths (~0.5 – 29 m), and thicknesses (~11 – 91 km). The volumes and flow masses range from ~1 – 430 km^3 and ~10^{11} – 10^{14} kg, respectively. Using three different models, we calculated a range of eruption rates (0.2 – 3.5 x 10^4 m^3/s), viscosities (10^4 – 10^7 Pa s), yield strengths (800 – 10^4 Pa), and emplacement times (14 hours – 22 years). While the flow lengths and volumes are typically larger than terrestrial lava flows by an order of magnitude, rheologies and eruption rates are similar based on our findings. Emplacement times suggest that eruptions were active for long periods of time, which implies the presence and persistence of open subsurface pathways. Differences in flow morphology and emplacement conditions across localities within Tharsis highlight different pathways and volumes of available material between the central volcanoes and the plains. The scale of the eruptions suggests there could have been eruption-driven local, regional, and perhaps, global impacts on the Martian climate. The relatively recent age of the eruptions implies that Mars has retained the capability of producing significant localized volcanism.

Plain Language Summary

Volcanoes have resurfaced a majority of the Martian surface. Understanding the volcanic history of Mars is critical to understanding the evolution of the planet. Lava flows are one of the most common volcanic features on Mars, and numerous examples are present in the Tharsis

volcanic province on shield volcanoes and in vast volcanic plains. Using three different approaches, we characterized the eruption conditions of 40 lava flows. In addition, we measured their dimensions and calculated volumes and masses. We observed flow dimensions (e.g. lengths and volumes) larger than typical terrestrial lava flows. Viscosities and yield strengths were similar to terrestrial values; however, effusion rates were generally at the higher end of terrestrial rates. These results indicate that lava flows erupted on Mars did not require exotic compositions or exceptionally high eruption rates to be emplaced. However, this does imply longer eruption times which requires the existence of long-lived subsurface conduits capable of transporting magma to the surface.

1. Introduction

Volcanism is a fundamental geologic process that has created and shaped the surfaces of the terrestrial planets in our solar system [*Carr,* 1973; *Carr,* 1974; *Greeley and Spudis,* 1981; *Wilson and Head*, 1983; *Pieri et al.*,1984; *Gregg and Fink*, 2000; *Plescia*, 2004; *Werner*, 2009; *Spudis et al.*, 2013]. The volcanic history of a planetary body provides information on its formation and evolution [*Carr,* 1973; *Carr,* 1974; *Greeley and Spudis*, 1981; *Wilson and Head,* 1983; *Spudis et al.*, 2013]. For Mars, where ~60% of the crust has been resurfaced by effusive volcanism, a variety of volcanic landforms have been preserved at the surface, including vast lava flow plains, sinuous rilles, massive shield volcanoes, cinder cones, and ash shields [*Carr,* 1974; *Greeley and Spudis*, 1981; *Plescia,* 2004; *Werner*, 2009; *Hauber et al.*, 2011; *Hiesinger et al.*, 2009; *Xiao et al*., 2012]. The bulk of Martian volcanism appears to have occurred early in the planet's history (>3Ga), with decreasing volcanic fluxes through time [*Werner,* 2009; *Tanaka et al.*¸2014]. Despite an abundance of volcanic features on Mars, the volcanic history of the planet remains complicated due to the lack of global compositional data, the lack of human observation during volcanic activity, and sometimes a lack of analogous terrestrial terrain and processes.

Using flow morphology to estimate eruption conditions has been a goal of terrestrial and planetary volcanology for decades and has fueled a number of studies [e.g., *Wilson and Head,* 1983; *Fink and Griffiths,* 1990; *Gregg and Fink,* 1996; *Cashman et al.*, 1998; *Glaze and Baloga,* 2006; *Hiesinger et al.*, 2007; *Baloga and Glaze*, 2008; *Hauber et al.*, 2011]. In the absence of direct observations, the eruption conditions and flow properties can be estimated based upon the morphology of preserved deposits. These deposits provide a snapshot into the planet's interior and composition. Previous studies have estimated lava flow eruption rates, viscosities, yield

strengths, and emplacement times using combinations of simplified fluid mechanics, numerical models, deposit morphology, and morphometry [e.g. *Griffiths and Fink*, 1992; *Gregg and Fink*, 1996; *Glaze and Baloga*, 2006; *Baloga and Glaze*, 2008; *Glaze et al.*, 2009; *Hauber et al.*, 2011; *Hiesinger et al.*, 2009].

In this study, we have observed and quantified the morphology and dimensions of 40 lava flows in the Tharsis Volcanic Province on Mars in order to calculate eruption rates, viscosities, yield strengths, and emplacements times. These 40 lava flows occur in the volcanic plains and in proximity to or on central volcanoes. High resolution images up to 0.4 m/pixel and digital terrain models at ~50 – 70 m/ pixel have enabled detailed analyses of these lava flows [*Jaumann* et al., 2007; *Malin* et al., 2007; *McEwan* et al., 2007]. We have applied three lava flow emplacement models that utilize flow morphology and morphometry to constrain eruption rates, rheology, and emplacement times, and compared those results to a wide range of analogous terrestrial data. The suite of models consists of 1) a standard cooling-limited rheologic treatment outlined in *Hiesinger et al.* [2007]; 2) the utilization of the non-dimensional parameter Ψ derived from laboratory analogue experiments; and 3) the self-replication model outlined in *Baloga and Glaze* [2008]. The calculated volumes, eruption rates, viscosities, and emplacement times are interpreted in terms of their implications for the eruption conditions of relatively recent volcanic activity on Mars and the subsurface pathways that transport magma in the Martian crust. An application of this method to lava flows on other volcanic bodies, such as Io or Venus, could also prove useful.

2. Background

The eruption conditions of lava flows on Mars have implications for understanding its composition, interior, and evolution. The morphology of terrestrial and extraterrestrial lava

flows has long been used as a proxy for the eruptive conditions at the time of emplacement [e.g., Walker 1971, 1973; *Carr*, 1973, 1974; *Wilson and Head*, 1983; *Griffiths and Fink*, 1992; *Gregg and Fink*, 1996; *Cashman et al.*, 1998; *Bleacher et al.*, 2007; *Hiesinger et al.*, 2007; *Baloga and Glaze*, 2008; *Hauber et al.*, 2011]. A number of studies have used the morphology and morphometry of lava flows on Mars to estimate effusion rates, viscosities, and yield strengths by applying cooling limited and rheologic models [*Wilson and Head*, 1983; *Glaze and Baloga*, 2006; *Bleacher et al.*, 2007; *Hiesinger et al.*, 2007; *Hauber et al.*, 2011]. These studies have necessarily made a variety of simplifying assumptions about lava flow rheology, composition, and environmental conditions during emplacement. Some studies have invoked either exceptional eruption rates never observed in terrestrial lava flows or exotic compositions to explain the very large dimensions of Mars lava flows [e.g., *Wilson and Head*, 1983; *Cashman et al.*, 1998 and references therein; *Garry et al*., 2007; *Giacomini et al.*, 2009]. These analyses were partly predicated on the following assumptions: the length of lava flows is controlled exclusively or largely by eruption rate; the entire flow front is active at all times with the flow moving as a coherent mass; and/or lava behaves as a Newtonian fluid [*Nichols*, 1939*; Bruno et al.*, 1996; *Baloga et al.*, 1998; *Baloga and Glaze*, 2008]. Although studies have demonstrated a Newtonian rheology may be assumed for the hot interior of a lava flow, *Hulme* [1976] demonstrated that the behavior of lava flows on Olympus Mons, Mars, and elsewhere, were better approximated by a Bingham rheology due to the significant yield strength of most lavas, particularly as they propagate and cool. Subsequent studies followed suit [e.g. *Bruno et al.*, 1996; *Hiesinger et al.*, 2007; *Glaze and Baloga*, 2006; *Baloga and Glaze*, 2008; *Hauber et al.*, 2011]. Recent works have accounted for more complex processes that occur during the emplacement of lava flows such as levee construction and overspills [*Baloga et al.*, 1998; *Baloga*

and Glaze, 2008; *Glaze et al.*, 2009]. Most studies aimed at constraining lava composition and effusion rates on Mars have focused on the Tharsis and Elysium volcanic provinces where some of the best-preserved lava flows on the planet are located. Due to dust cover, however, compositional data is sparse to nonexistent in these localities [*Christensen*, 1986; *Hiesinger et al.*, 2007; *Baloga and Glaze*, 2008; *Hauber et al.*, 2011; *Rogers and Christensen*, 2007]. However, a basaltic to basaltic andesite composition of much of the Martian crust has been determined using thermal infrared spectral measurements of less dust covered regions [*Rogers and Christensen*, 2007]. Based on the moderate range of compositions observed in the dust-free regions, it is likely that the Tharsis region is basaltic as well.

Laboratory analogue experiments have provided a fundamental understanding of lava flow emplacement processes and their relationship to propagation rate and morphology, and have thus been used to make predictions of lava flow behavior on other planets [*Fink and Griffiths*, 1990; *Griffiths and Fink*, 1992; *Gregg and Fink*, 1996; 2000; *Blake and Bruno*, 2000; *Soule and Cashman*, 2004; *Rader et al.*, 2017; *Peters*, 2020]. Previous laboratory studies have examined lava flow morphologies by extruding substances analogous to lava into controlled environments under controlled source conditions [*Fink and Griffiths*, 1990, 1992; *Gregg and Fink*, 1996, 2000]. Polyethylene glycol (PEG) wax has been demonstrated to be a useful analogue to real lava flows due to its temperature dependent viscosity and timescale of surface crust formation [*Fink and Griffiths*, 1990, 1992; *Gregg and Fink*, 1996, 2000; *Soule and Cashman*, 2004]. *Fink and Griffiths* [1990] derived a dimensionless parameter, Ψ, which is a ratio of the characteristic time scale of crust formation, which is controlled by surface cooling, to the characteristic time scale of lateral thermal advection, for which flow propagation rate is a proxy.

Fink and Griffiths [1990] observed five morphologies produced in the laboratory: no crust, levees, folds, rifts, and pillows, which occur on a continuum from high to low Ψ values, respectively (Fig. 1). Analogous morphologies have been observed in nature [*Fink and Griffiths,* 1990, 1992; *Griffiths and Fink,* 1992; *Gregg and Fink,* 1996]. Subsequent studies utilized PEG experiments to address slope effects [e.g., *Gregg and Fink,* 2000]. Extrapolating laboratory experiments to other terrestrial bodies such as Mars has been attempted in order to constrain eruption parameters and predict expected morphologies, although the image resolution at the time of these studies was limited to >150 m/pixel [*Fink and Griffiths,* 1992; *Gregg and Fink,* 1996; *Peters,* 2020]. Laboratory experiments, in conjunction with rheologic modelling and remote sensing geomorphology, therefore provide an additional constraint on prehistoric eruption conditions on Mars.

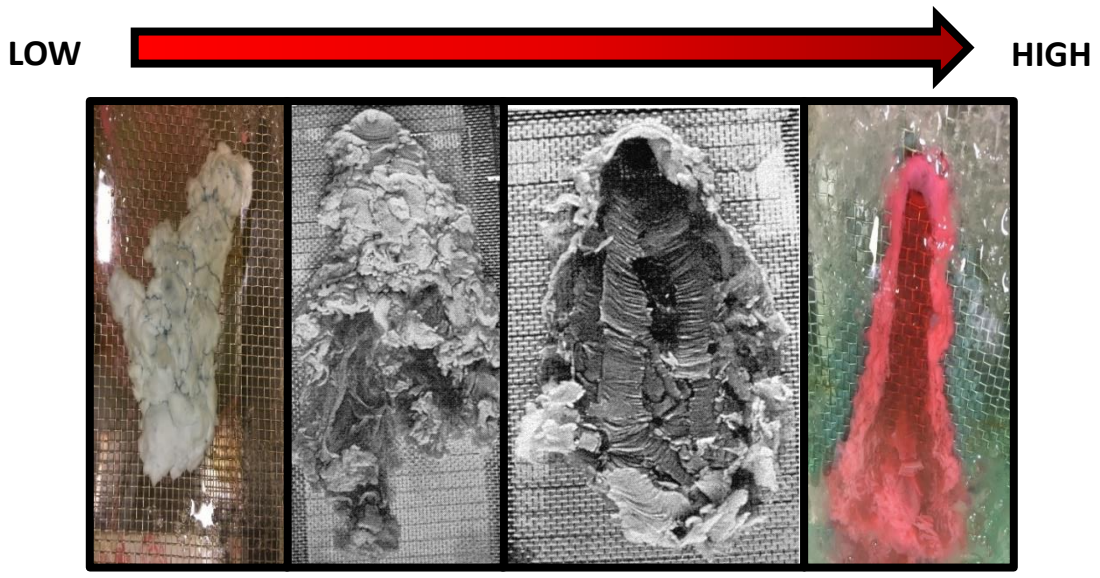

Figure 1: Examples of the four primary morphologies observed by *Fink and Griffiths* [1990], *Gregg and Fink* [2000], and *Peters* [2020]. From low to high Ψ, the morphologies are Pillows, Rifts, Folds, and Levees. Modified from Gregg and Fink, 2000.

3. Geologic Setting

3.1. Tharsis Volcanic Province

The Tharsis region represents the largest volcanic province on Mars (Fig. 2), containing the tallest volcano in the solar system (Olympus Mons at ~22 km), one of the largest volcanoes on the planet in areal extent (Alba Mons at ~1.15 x 10^6 km^2), and the Tharsis Montes – three large shield volcanoes [*Carr*, 1973; *Carr*, 1974; *Crumpler and Aubele*, 1978; *Greeley and Spudis*, 1981; *Scott and Tanaka*, 1981; *Plescia*, 2004]. In addition, the region contains innumerable lava flows and small shields, in what is sometimes characterized as plains-style volcanism [*Greeley*, 1977; *Baloga and Glaze*, 2008; *Glaze et al.*, 2009; *Hiesinger et al.*, 2007; *Hauber et al.*, 2011]. Tharsis dominates the western hemisphere of the planet and occupies a region from ~60° N to ~40° S and 210° E to 300° E and ~4000 x 6000 km. Volcanic activity began ~4 Ga and has occurred within the last ~100 Ma [*Carr*, 1973; *Carr*, 1974; *Scott and Tanaka*, 1981; *Plescia*, 2004; *Werner*, 2009]. The 40 lava flows featured in this study occur throughout the Tharsis Volcanic Province, primarily on and around Olympus Mons, in the volcanic plains surrounding the Tharsis Montes, and Daedalia Planum. A brief summary is given of each region.

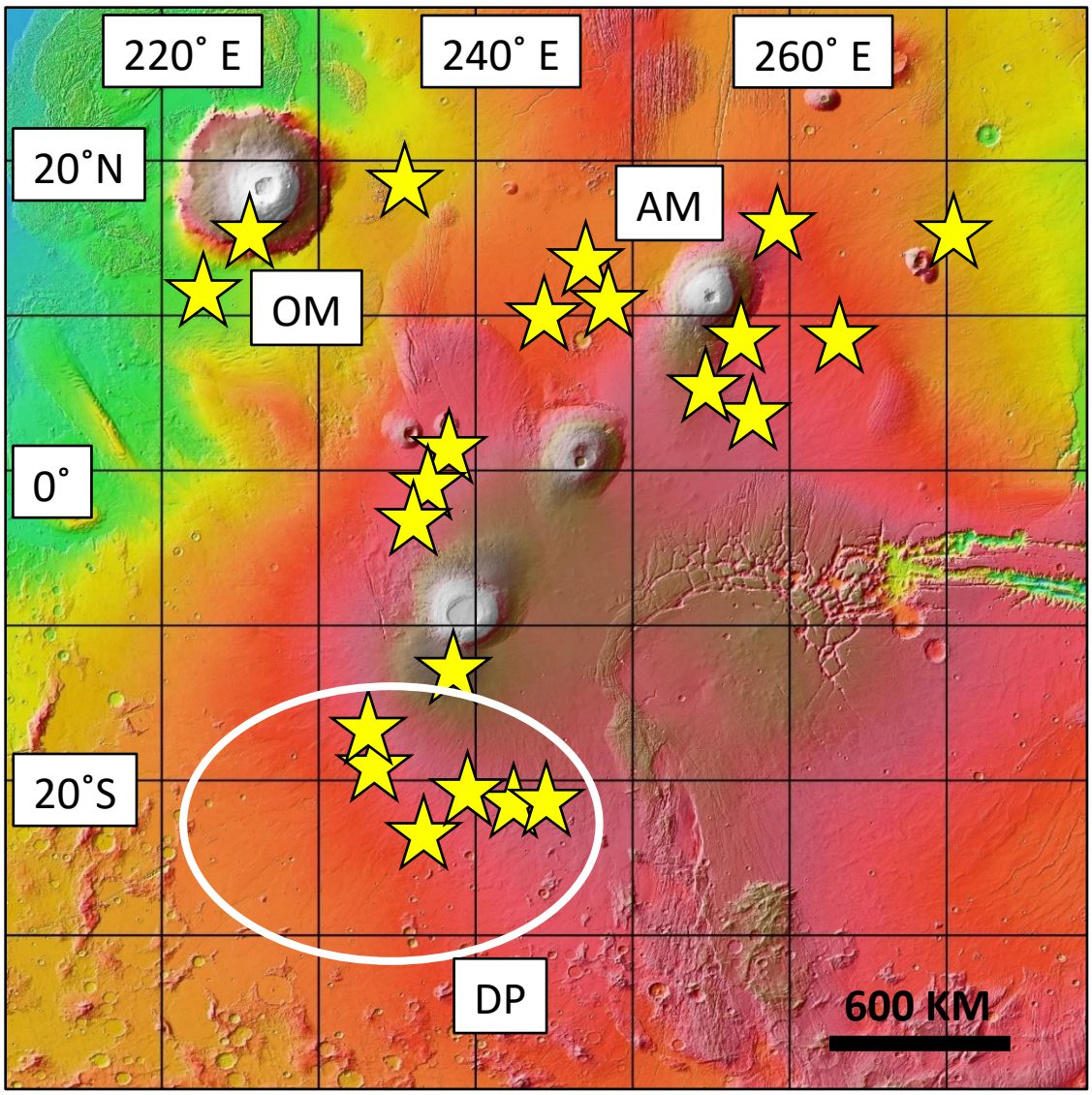

Figure 2: Map of study area, the Tharsis Volcanic Province. Base map is MOLA colorized topography, with warm colors representing areas of higher elevation. Square label demarks Olympus Mons (OM) and Ascraeus Mons (AM), while white circle encompasses Daedalia Planum (DP).

3.1.1. Olympus Mons & Ascraues Mons

Olympus Mons and Ascraues Mons are two large shield volcanoes in the Tharsis volcanic province. Olympus Mons is 600 km across and 22 km high and Ascraues Mons is 400 km across and 15 km high. Olympus Mons and is situated northwest of the Tharsis Montes and southwest of Alba Mons (Fig. 2), while Ascraeus Mons (located east of Olympus Mons) is the

188 northernmost of the Tharsis Montes [*Carr*, 1973; *Greeley and Spudis*, 1981; *Plescia*, 2004;
189 *Werner*, 2009]. Both volcanoes display nested caldera complexes and evidence of widespread
190 effusive eruptions. Extensive dust cover prohibits compositional analyses of either volcano, but
191 both volcanoes are morphologically similar to Hawai'i and the Galapagos shield volcanoes and a
192 basaltic composition has been inferred for their erupted lavas [e.g., *Christensen*, 1986; *Bleacher*
193 et al., 2007; *Byrne et al*., 2012; *Rogers and Christensen*, 2007]. Both volcanoes display gentle
194 sloping flanks (~4 – 6˚) with some steepening on the upper flanks [e.g., *Plescia*, 2004].
195 Although construction of Olympus Mons and Ascraeus Mons is believed to have been largely
196 completed by the Late Noachian or Early Hesperian (>3.6 Ga), their surfaces have been dated to
197 ~100 – 800 Ma based on crater count modeling [e.g. *Neukum* et al., 2004; *Werner*, 2009; *Xiao et*
198 *al*., 2012]. Some of the youngest features on Olympus Mons and Ascraeus Mons include lavas
199 on the floors of the nested calderas (~100–200 Ma), some flank lava flows (~50 Ma), and small
200 satellite vents and arcuate graben [e.g., *Neukum* et al., 2004; *Werner*, 2009; *Byrne et al*., 2012;
201 *Tanaka et al*., 2014; *Peters and Christensen*, 2017].

202 3.1.2. Volcanic plains & Daedalia Planum

203 Volcanic plains formed by countless overlapping lava flows cover much of the terrain
204 within the Tharsis Volcanic Province (Fig. 2) producing a monotonous topography of gentle
205 slopes, punctuated by low shields, cinder cones, graben, and the central volcanoes [e.g., *Carr*,
206 1973, 1974; *Greeley and Spudis*, 1981; *Hauber et al.*, 2011]. Individual lava flows can extend
207 hundreds of kilometers from their sources, which include dozens of low shield volcanoes, the
208 Tharsis Montes, and buried sources [*Carr*, 1973, 1974; *Crumpler and Aubele*, 1978; *Greeley and*
209 *Spudis*, 1981; *Hiesinger et al.*, 2007; *Baloga and Glaze*, 2008; *Glaze et al.*, 2009; *Hauber et al.*,
210 2011]. Daedalia Planum – an example of this terrain – is an 18 x 10^6 km^2 volcanic plain on Mars

located southwest of Arsia Mons, one of the Tharsis Montes [*Plescia,* 2004; *Werner*, 2009; *Giacomini et al.,* 2012]. It too hosts very long lava flows (>200 km in some cases), with many believed to be sourced by activity related to Arsia Mons, the southernmost and oldest of the Tharsis Montes [e.g., *Scott and Tanaka,* 1981; *Plescia,* 2004; *Giacomini et al.,* 2009, 2012; *Werner,* 2009; *Crown and Ramsey,* 2016]. Recent studies on Daedalia Planum have measured average lava flow thicknesses of 35 – 70 m using high resolution image and elevation data, observed inflation in lava flows using possible lava rises and tumuli, and attempted compositional analysis via spectral mapping [e.g., *Giacomini et al.,* 2009, 2012].

4. Methodology

4.1. Datasets & Analyses Criteria

We used image data from the Mars Reconnaissance Orbiter (MRO) Context Camera (CTX: ~5 m/pixel), [*Malin* et al., 2007], the Mars Odyssey Thermal Emission Imaging System in the infrared (THEMIS IR: 100 m/pixel), [*Christensen* et al., 2004], and the MRO High Resolution Imaging Science Experiment (HiRISE: ~0.5 m/pixel) instruments [*McEwan* et al., 2007]. We utilized topographic data from the Mars Global Surveyor (MGS) Mars Orbital Laser Altimeter (MOLA: ~463 m/pixel) digital elevation model (DEM) [*Zuber* et al., 1992] dataset, as well as Mars Express High-Resolution Stereo Camera (HRSC) DEM (DEM cell size: 50 – 75 m) [*Jaumann* et al., 2007]. While the Tharsis region has extensive CTX and localized HiRISE coverage, high resolution HRSC DEMs did not cover the entire study area. As a result, some flows were characterized using the MOLA DEM [e.g., *Glaze et al*., 2003]. Due to the resolution of the MOLA DEM, larger lava flows were given priority when HRSC DEM coverage was not available. All datasets were accessed and analyzed using the Java Mission Planning and Remote Sensing (JMARS) GIS software [e.g., *Gorelick et al.,* 2003].

For this study, we considered lava flows in the Tharsis Volcanic Province because of the large number of well-preserved flows and extensive overlapping datasets. We selected 40 lava flows based on the following criteria: 1) morphology and 2) data coverage. We prioritized flows with relatively unobstructed flow along their lengths and relatively well-defined margins. In all cases, the full extent of the original flow was not preserved due to superimposed lava flows, impact craters, or erosion/degradation. These processes reduced the available flow area for study and also resulted in the erasure of the flow source. As a result, our flow lengths, volumes, and volumetric flow rates represent minima. We also prioritized lava flows with adequate data coverage. Every selected lava flow had CTX visible image coverage and at least partial HRSC and/or MOLA DEM coverage. Despite the ~1 m dust mantle that blankets the Tharsis Volcanic Province, lava flow surface texture is relatively well preserved and discernible [*Christensen*, 1986]. Compression ridges are visible on a number of lava flows, owing to the resilience of these features in the face of erosion, degradation, and dust cover. However, finer scale morphologies, such as pahoehoe lava lobes (which tend to be meter-scale features), if originally present, are not visible due to limited spatial resolution. Overall, the morphologies and morphometric properties of lava flows in the Tharsis Volcanic Province suggest a basalt to basaltic andesite composition [e,g., *Carr*, 1974; *Hulme*, 1974; *Bleacher et al.*, 2007; *Hiesinger et al.*, 2007]. We measured and calculated the length, mean width, mean thickness, surface area, volume, and mean slope for each of the 40 lava flows in this study (Table 1). The length of each flow was measured using a centerline. The mean width and thickness of each flow were calculated using multiple cross-sectional profiles. We calculated the volume by multiplying surface area by mean thickness. We applied the three models discussed above to the 40 lava flows in this study in order to estimate volumetric flow rates, bulk viscosities and yield strengths,

and emplacement times. The models and how they were applied to the data set are detailed in the following section.

	Lat (N)	Long (E)	Region	Length (km)	Mean Width (km)	Flow Thickness (m)	Volume (km^3)	Observed Ψ Morphology
Flow 1	18.53	235.94	E of Olympus Mons	21	5.61	10.5	1.32	Levee (fed by)
Flow 2	11.914	244.629	Tharsis	313	18.3	46	281.80	Levees
Flow 3	14.504	248.246	Tharsis	314	28.8	39	436.18	Smooth-Levees
Flow 4	15.199	226.654	Olympus Mons	18.3	0.592	27	0.38	Levee-Folds
Flow 5	15.008	226.823	Olympus Mons	33	0.57	11.5	0.25	Levee-Folds
Flow 6	15.761	224.764	Olympus Mons	19	3	25	1.48	Levees
Flow 7	11.739	224.015	S Olympus Mons	100	6.9	26	23.40	Levees
Flow 8	11.597	222.495	S Olympus Mons	41	6.5	14	1.76	Levees
Flow 9	-19.332	243.262	Daedalia Planum	78	5.9	25	12.00	Levee
Flow 10	-20.945	240.957	Daedalia Planum	136.5	5.89	33	34.16	Levee
Flow 11	-21.733	242.555	Daedalia Planum	58	16.3	35.5	38.41	Levee-Folds
Flow 12	-23.297	242.812	Daedalia Planum	266	19.3	45	268.16	Levees
Flow 13	-22.547	244.16	Daedalia Planum	201	11.8	30	101.07	Levees
Flow 14	-23.195	237.617	Daedalia Planum	219	6	32	52.22	Levee
Flow 15	-19.081	234.684	Daedalia Planum	92	3.8	15	6.11	Levee-Folds
Flow 16	-17.307	233.48	Daedalia Planum	164.5	3.23	16	12.24	Levees
Flow 17	-22.665	237.6084	Daedalia Planum	106	4.48	17	10.17	Levees
Flow 18	8.945	257.408	Ascraeus Mons	16	4.1	15	0.99	Folds
Flow 19	15.521	261.191	Ascraeus Mons	78.5	4.19	23	8.33	Levees
Flow 20	12.102	250.046	W of Ascraues Mons	99	12	37	65.38	Levees
Flow 21	11.193	248.41	W of Ascraues Mons	121	16.5	38	73.07	Smooth-Levees
Flow 22	15.757	225.213	Olympus Mons	15	1.15	17.5	0.33	Levees
Flow 23	15.814	225.379	Olympus Mons	30.4	5.93	91	8.20	Rifts
Flow 24	15.156	225.105	Olympus Mons	27.12	1.32	18	0.77	Levee
Flow 25	14.997	225.298	Olympus Mons	59.5	6.79	68	13.74	Rifts

Flow 26	16.089	227.269	Olympus Mons	13.3	3.72	64	1.58	Rifts
Flow 27	15.91	227.239	Olympus Mons	27.6	2.2	37	1.12	Rifts
Flow 28	15.178	259.464	Ascraeus Mons	47.6	4.6	30.8	3.37	Rifts
Flow 29	15.689	259.131	Ascraeus Mons	29	7	38.4	3.90	Rifts
Flow 30	8.572	263.609	Tharsis	43.7	7.13	29	8.96	Levee
Flow 31	-12.934	239.423	Daedalia Planum	25.3	2.08	31	1.72	Levee
Flow 32	-0.879	237.326	Tharsis	77.2	5.94	30.5	15.16	Levee
Flow 33	-3.006	239.936	Tharsis	69.3	6	29	11.66	Levee
Flow 34	16.210	261.309	Tharsis	72	3.67	25	7.13	Levee
Flow 35	5.018	256.914	Tharsis	98.6	3.11	16	5.09	Levee
Flow 36	5.229	254.687	Tharsis	23	1.26	11	0.46	Levee
Flow 37	5.371	255.546	Tharsis	38.4	1.86	13	1.09	Levee
Flow 38	3.576	259.678	Tharsis	128	4.94	18.1	11.91	Levee
Flow 39	1.347	238.558	Tharsis	71.1	6.7	23	12.03	Levee
Flow 40	15.51	271.857	Tharsis	219	13.8	55	173.69	Levee

259 **Table 1:** Data on 40 lava flows in Tharsis volcanic province on Mars investigated in this study.

260 4.2. Models for interpreting the datasets

261 4.2.1. *Cooling-limited and Rheologic Model*

262 We applied a standard rheologic treatment to 34 of 40 lava flows using methods outlined
263 by *Hiesinger et al.* [2007], and references therein, to calculate eruption rate and viscosity. Six of
264 40 lava flows were excluded because they exhibit prominent ridges likely formed through
265 repeated overspills from a channel or tube during emplacement, in stark contrast to the typical
266 flows for which this method was intended [*Sakimoto et al.*, 1997]. The method uses 1) the
267 Graetz number (G_z), a dimensionless number that characterizes the ratio of the time scale of
268 cooling by conduction at the edges or surface of the flow, to that of fluid advection downstream;
269 and 2) Jefferey's equation, which is a steady-state momentum equation reduced to a force
270 balance between downslope gravitational forces that drive the flow and viscous forces that
271 impede the flow, can be expressed in terms of flow velocity, geometry, and fluid viscosity
272 [*Jeffreys*, 1925; *Wilson and Head*, 1983]. This approach requires some assumptions including:
273 laminar flow of a Newtonian fluid; steady-state emplacement at low velocities; flow dimensions
274 that reflect rheological properties of the flow [e.g., *Wilson and Head*, 1983; *Hiesinger et al.*,
275 2007; *Hauber et al.*, 2011]; and a Graetz number of ~300 that defines when the flow halts,
276 following *Pinkerton and Sparks* [1976].

277 According to a suite of observations of cooling-limited lava flows at Mt. Etna, *Pinkerton*
278 *and Sparks* [1976] found that flows ceased advancing at G_z of approximately 300, when crust
279 extent and strength was sufficient to prevent the continued propagation of the small amount of
280 melt remaining in the core of the flows. *Gues*t et al. [1987] questioned the value of 300 because
281 *Pinkerton and Sparks* [1976] did not take into account branching of lava flows or the possibility
282 of volume-limited flows. However, for cooling-limited flows, Guest et al. [1987] place the

283 halting Graetz number at approximately 230, very close to the assumed value of 300. The Mars
284 flows studied here exhibit limited to no branching, and given their large volumes (see below),
285 they were unlikely to have been volume-limited. We therefore assume that they were cooling-
286 limited and proceed with a halting Graetz number value of 300. Graetz number (G_z) can be
287 expressed as
288
289 $$G_z = [Q/(\kappa x)]\ (w/h) \qquad \text{(Eq. 1)}$$
290
291 where Q is the effusion rate, κ is thermal diffusivity of the lava which is a function of its
292 composition ($m^2\ s^{-1}$), x is flow length, w is mean flow width (Table 1), and h is mean flow
293 thickness (Table 1) [*Wilson and Head*, 1983]. This equation is a modification of the original
294 Graetz number for cooling of a fluid in a cylindrical pipe. Eq. 1 accounts for the fact that thinner
295 flows cool faster than deeper flows by including the aspect ratio w/h [*Hulme and Fielder*, 1977].
296 Here effusion rate, Q, was obtained by rearranging Eq. 1, assuming a halting Graetz number of
297 300, using the flow geometries measured from the previously described data sets (Table 1), and
298 applying the thermal diffusivity of basalt, $5.00 \times 10^{-7}\ m^2/s$ [e.g., *Wilson and Head,* 1983; *Hon et*
299 *al.,* 1994; *Pasckert et al.,* 2012].
300 Jeffrey's equation can be used to relate the effusion rate of a flow to its viscosity, density,
301 and flow dimensions. It is derived for flow on an infinitely wide plane and is written as follows
302 for broad flows [*Jeffreys*, 1925].
303
304 $$\eta = \rho g h^3 w \sin\alpha\ /3\mathrm{Q} \qquad \text{(Eq. 2)}$$
305

where η is the effective dynamic viscosity of the flow during emplacement and propagation, ρ is the lava density during emplacement, *w* and *h* are the flow dimensions as described previously, Q is volumetric effusion rate, α is the underlying slope, and 3 is a constant used for flows that are much wider than they are deep [*Jeffreys*, 1925]. We assumed a density of 2700 kg/m^3 which is consistent with estimates from previous studies and within the range of terrestrial basalt values [e.g., *Rowland et al.*, 2004; *Hiesinger et al.*, 2007; *Hauber et al.*, 2011; *Pasckert et al.*, 2012]. Q from Eq. 1, along with flow geometry, underlying slope, and magma density were used in Eq. 2 to calculate dynamic viscosity η. Emplacement times were estimated from Q and measured individual flow volumes.

4.2.2. *Laboratory experiments and Ψ*

We classified each of the 40 observed lava flows by dominant surface morphology, which corresponds to a particular Ψ regime [*Fink and Griffiths,* 1990; *Gregg and Fink,* 1996]. Ψ is a powerful way of understanding the dynamics of flow emplacement using only flow morphology. Because it is a dimensionless parameter, Ψ can be applied to flows of any composition, rheology, and scale so long as reasonable emplacement constraints such as ambient conditions and properties of the flowing liquid can be assumed. Five flow morphologies corresponding to discreet Ψ ranges have been observed. Those morphologies from high to low, Ψ >55 to Ψ ~1, are: No Crust, Levees, Folds, Rifts, and Pillows (Fig. 1) [*Fink and Griffiths,* 1990, 1992; *Gregg and Fink,* 2000]. Transitional morphologies are also observed in the lab and on Mars, demonstrating that the morphologies are produced on a continuum. And, as stated previously, the textures observed in the laboratory are observed in nature – from terrestrial felsic lava flows to sulfur flows [e.g., *Fink et al.*, 1983; *Pieri et al.*, 1984; *Griffiths and Fink,* 1992; *Gregg and Fink*, 1996; *Peters*, 2020].

In the analysis presented, we assumed that the predominant morphology observed represents the dominant Ψ regime during the time of emplacement (Fig. 1). The validity of this assumption has been demonstrated in the laboratory to the extent possible [*Fink and Griffiths,* 1990, 1992; *Gregg and Fink,* 2000]. Although there exists the possibility that flows pass through a number of morphological regimes throughout the emplacement process, the final morphology preserved in the rock record is the only source of data we have for the surface of Mars. We proceed with this caveat in mind, and thus assume that our calculations based on Ψ regime best represent the dominant flow emplacement conditions. Furthermore, each flow was assigned a Ψ value range corresponding to the observed morphology. Some transitional morphologies (i.e. levee-fold) were observed, while no pillow morphologies were definitively observed. We interpreted the lava ridges, previously observed on Olympus Mons, Alba Mons, and other localities, and interpreted as lava tubes [*Sakimoto et al.,* 1997; *Bleacher et al., 2007*], to represent rift morphology. Our interpretation is based on laboratory analogue experiments using PEG wax performed on slopes, which yielded ridge-like structures produced by lava tubes [*Peters,* 2020].

Ψ can be written in terms of a modified Peclet number, Π, a non-dimensional cooling timescale for the crust, τ_s, and a ratio of temperature differences including ambient, solidification, and wax or lava temperatures, θ_s [*Fink and Griffiths*, 1990, Eq. 10].

$$\Psi = \Pi \tau_s(\theta_s) \quad \text{(Eq. 3)}$$

Π incorporates the traditional Peclet number (Pe), which is the ratio of the rate of advective heat transport by the flowing lava to the rate of conductive heat transport at the flows surface. Π also includes the effects of reduced gravity (g'), kinematic viscosity (ν), thermal

diffusivity of the wax or lava (κ), and the timescale (λ) over which the contact temperature of the wax or lava reaches the temperature of the ambient environment far from the lava surface, where the contact temperature is defined as the temperature at the interface between wax or lava and the ambient.

$$\Pi = \left(\frac{g\prime}{\nu}\right)^{\frac{2}{3}} \kappa^{\frac{1}{3}} \lambda Pe^{\frac{1}{3}} \quad \text{(Eq. 4)}$$

Like Pe, Π represents a ratio of a characteristic advective flux or flow rate downstream to a characteristic thermal diffusion rate at the surface of the flow [*Fink and Griffiths*, 1990, Eq. 11].

Ψ can also be written as a ratio of the solidification and advection time scales, which is more descriptive.

$$\Psi = \frac{t_s}{t_a} \quad \text{(Eq. 5)}$$

Here, t_s represents the timescale of solidification of the surface crust and t_a represents the timescale of horizontal advection. Using the relationships in Eq. 3 and 4, we can calculate a range of effusion rates corresponding to the Ψ ranges for each flow morphology, for assumed Mars eruption and ambient conditions. From those effusion rates and measured flow volumes, we can also calculate a range of emplacement times for each flow.

However, in order to translate the Ψ ranges to eruption rates, we are required to make simplifying assumptions about the ambient environment and the erupted liquid. In the lab, the

ambient environment corresponds to the chilled bath or a sucrose solution and the erupted fluid refers to the PEG wax. For Mars, these values correspond to the ambient environment of the Martian surface and the lava flow. We assumed that radiation is the primary way a lava flow loses heat on Mars based on previous work, which found that radiant heat loss is an order of magnitude greater than that for convection or conduction [e.g., *Griffiths and Fink*, 1992; *Gregg and Fink,* 1996; *Rowland et al.*, 2004]. As a result, convective and conductive losses are considered to be negligible. In addition to the flow properties mentioned previously (i.e. density, thermal diffusivity), we assumed an ambient environment temperature of 210 K, an atmospheric density of 0.02 kg/m^3, a solidification temperature of 900˚C, and gravity of 3.71 m^3/s [e.g., *Peck*, 1978; *Rowland et al.*, 2004]. The ambient environment temperature, atmospheric density, and gravity represent the average values for Mars [e.g., *Rowland et al.*, 2004] and deviations of these values do not significantly impact our results. For values related to the Martian atmosphere, specifically kinematic viscosity, we assumed pure CO_2 [*Chemical Rubber Company*, 1984; *Crane Company*, 1988]. The basalt solidus is cited as 980˚C; however, the internal temperature of barely mobile basalt flows has been measured at temperatures as low as 800˚C and basalt flows on Mt Etna have been typically modeled with solidification temperatures of ~870 ˚C [*Peck*, 1978; *Pinkerton et al.*, 2002; *Vicari et al.*, 2007; *Belousov et al.*, 2015]. We find a value of 900˚ C to be reasonable and within the range of previous studies. The solidification temperature has the largest impact on Ψ effusion rate estimates, with a deviation of ± 50˚ C yielding an order of magnitude difference. Lava density (2700 kg/m^3) had a similar impact, but only if changed by >25%. We assumed the lava flows in our study erupted at 1150˚C, which is similar to the erupted temperature of basalts at Hawaiian volcanoes and Mt. Etna and within the

range of typical terrestrial basalts [1100 – 1250˚C, *Pinkerton*, 1987; *Harris and Rowland*, 2001; *Vicari et al*., 2007; *Harris and Rowland*, 2015].

4.2.3. Self-replicating lava flow model

Many of the lava flows observed in the major Martian volcanic provinces of Tharsis and Elysium display a similar repetitive morphology. *Baloga and Glaze* [2008] termed these flows "self-replicating lava flows" and identified a set of defining criteria: morphologic characteristics that repeat over the length of the flow, relatively constant channel and levee dimensions, and a single channel that is visible for most of its length (Fig. 3). Their corresponding model of propagation takes into account mass removed from the active molten lava flow during the formation of lateral levees at the flow front as it propagates. The model assumes that levees are created at the flow front due to a vertical parabolic velocity profile in the molten core consisting of a Newtonian fluid, in which fluid at the top of the flow is traveling downslope faster than fluid at its base (Fig. 4) [*Glaze and Baloga*, 2006; *Baloga and Glaze*, 2008]. The total excess flow rate (Q_{ex}) that forms the levees is calculated as a product of the average excess flow velocity, (u_c), width of the channel, and the thickness of the nondeformable crust atop the flow [*Baloga and Glaze*, 2008, Eq. 10]. The excess mass is then left behind as the flow front advances at the average downstream velocity of the molten core (u_c). Only a subset of lava flows in this study – 13 of 40 – met the *Baloga and Glaze* [2008] criteria of self-replicating flows.

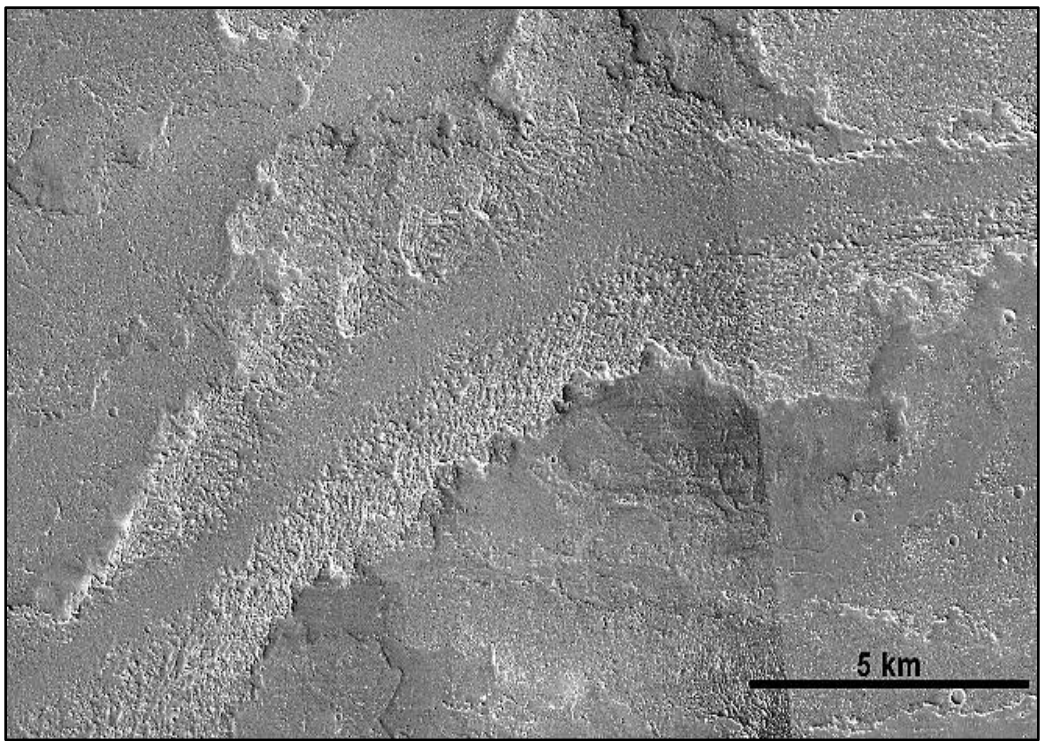

Figure 3: An example of a long, self-replicating lava flow in the volcanic plains of Tharsis south of Olympus Mons. The channel is clearly defined, has an approximately constant width, and levees are well developed and near constant width.

Using methods outlined in *Baloga and Glaze* [2008] and references therein, we calculated eruption rates (Q) and the resultant viscosities and emplacement times for the 13 qualifying lava flows across the Tharsis Volcanic Province. To do so, we first calculated the levee widths (w_l):

$$w_l = \frac{Q_{ex}}{u_c * h_l} \quad \text{(Eq. 6)}$$

where h_l is the levee thickness. Eq. (6) assumes that the excess volume flux Q_{ex} is u_c times the dimensions of the levees, h_l and w_l. The crust thickness is assumed to be the difference between total flow thickness and the liquid core thickness (h_c). The total flow thickness is approximated by the height of the levees, such that the crust thickness is $h_l - h_c$. Crust thickness was found as a

function of distance downstream and the data was smoothed as in *Baloga and Glaze* (2008) reaching an asymptotic value [Eqs. 12 & 13, Figure 8]. A cooling time for the asymptotic crust thickness to form was calculated using solidification by radiant cooling following *Hon et al.* [1994]. The emplacement duration of the flow was assumed to be the same as the time required for crustal growth. Average effusion rate was calculated for each flow using its total volume and the emplacement time.

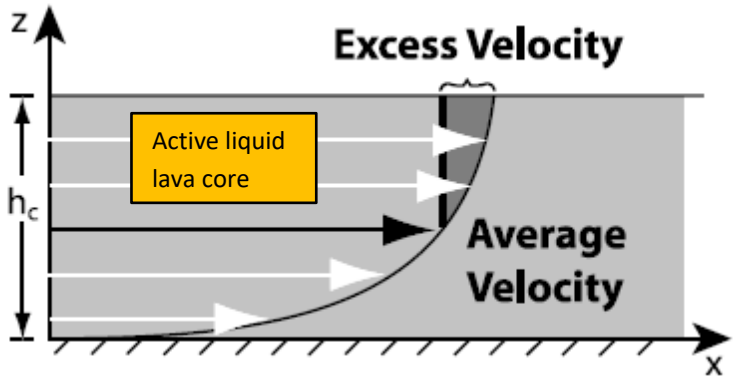

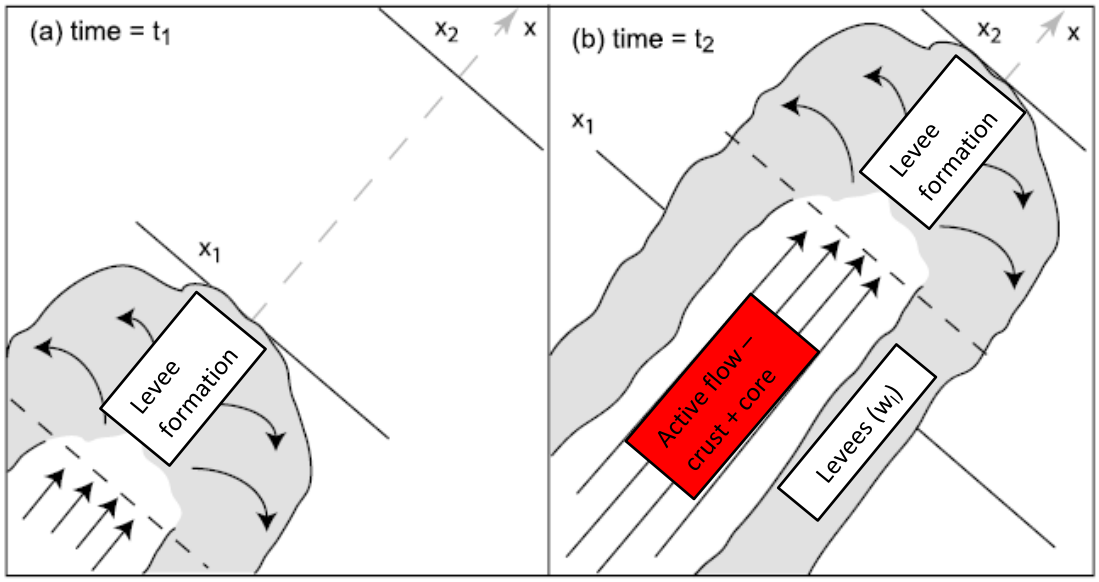

Figure 4: Modified from *Baloga and Glaze* [2008] illustrating how "self-replicating" lava flows, which include well-defined channels and levees of relative constant width, are produced. As the flow passes a given point, some mass of the flow at the flow front is deposited to form levees.

443 2.2.4 Yield strength calculation

444 Our use of Eqs. 1 and 2 above assume Newtonian behavior, allowing viscosity to be
445 calculated from Jeffrey's equation (Eq.2). However, many suggest that most lavas, especially
446 those cooling during emplacement, behave as Bingham fluids [e.g., *Moore*, 1978]. In order to
447 explore this rheology further, we estimate the yield strength (σ) of each flow using underlying
448 slope (α), flow thickness (h), and an assumed lava density of 2700 kg m^{-3} (following the
449 procedure of *Heisinger* et al. 2007 and references therein).

450

451 $$\sigma = \rho g \sin(\alpha) h \quad \text{(Eq. 7)}$$

452

453 **5. Results**

454 5.1. Classification of Qualitative Flow Morphologies

455 5.1.1. Channelized flows – high Ψ

456 Channelized lava flows – a common feature of either high-volume eruptions or flows
457 emplaced on steep slopes – are widely observed on the plains and shield volcanos of the Tharsis
458 volcanic province [e.g., *Carr*, 1973, 1974; *Greeley and Spudis*, 1981; *Baloga and Glaze*, 2008].
459 These flows are characterized by clearly defined (usually wide) channels and prominent levees
460 (Fig. 5a). The sources of these flows are obscured by the superposition of later flows and the
461 termination of the flow is marked by a reduction of channel visibility and the fanning out of the
462 flow into a smooth, featureless flow surface. Of the 40 lava flows in this study, 27 are
463 considered channelized flows. Thirteen of these flows display the self-replicating morphology
464 described in *Baloga and Glaze* [2008]. Channelized lava flows tend to be smaller in length and
465 width on central volcanoes than in the volcanic plains, and generally appear to correspond to the

high Ψ regime and, in the lab, are produced on slopes >5˚ or on shallower slopes at high eruption rates [*Peiterson and Crown*, 1999; *Gregg and Fink*, 2000; *Peters*, 2020].

5.1.2. Corrugated (folded) flows – intermediate Ψ

Corrugated flows – which are analogous to the fold morphology observed in PEG wax experiments performed in the laboratory – are a variation of channelized flows [*Fink and Griffiths*, 1990, 1992; *Gregg and Fink*, 2000]. Typically, these flows display a broad, open channel and clearly defined levees. However, the inside of the channel and terminus of the flow is characterized by a corrugated surface texture (Fig. 5b), interpreted to be the physical manifestation of compression ridges on the surface crust. This texture has also been observed on submarine and subaerial terrestrial flows. In this study, these flows are observed on Olympus Mons and in the volcanic plains surrounding Ascraeus Mons. Of the 40 lava flows observed in this study, five display this morphology. Of those five, four display a transitional morphology between channelized and corrugated flows. The same behavior has been observed in the laboratory and, in those cases, intermediate Ψ value ranges corresponding to transitional morphologies were assigned [*Fink and Griffiths*, 1990, 1992; *Gregg and Fink*, 2000].

5.1.3. Smooth flows – very high or low Ψ morphology

Many lava flows on Mars display a smooth, featureless texture that some believe represent sheet flows emplaced by high eruption rates and/or low viscosity lavas, although some of these flows might instead represent inflated pahoehoe flows [e.g., *Hon et al.*, 1994; *Bleacher et al.*, 2017]. In our study, we avoided entirely smooth lava flows due to an inability to distinguish between those flows which might represent wholesale emplacement at high eruption rates and those which might have been emplaced as pahoehoe flow fields that have undergone inflation. Nonetheless, two of the flows in our study, found in the volcanic plains, display

smooth textures along certain lengths of the flow. In these instances, a long-channelized portion of the flow is also observed, and we therefore interpret these flows as transitional between channelized and sheet flows corresponding to high / very high Ψ values.

5.1.4. Lava ridge flows – low Ψ on slopes

Lava ridges have been observed on and around central volcanoes, specifically Alba Mons, Olympus Mons, and in the apron associated with Ascraeus Mons [*Sakimoto et al.*, 1997; *Bleacher et al., 2007*]. These features have been interpreted as tube-fed flows, or lava tubes. Lava ridges generally produce a broad triangular shaped rise in cross-section. Skylights are observed on some of the ridges, where portions of the roof have collapsed into the void space below. We interpret the tube-fed flows as being associated with low Ψ values, since analogous features have been reproduced in the lab on a slope at low Ψ values. Six of the 40 studied flows are classified as lava ridges.

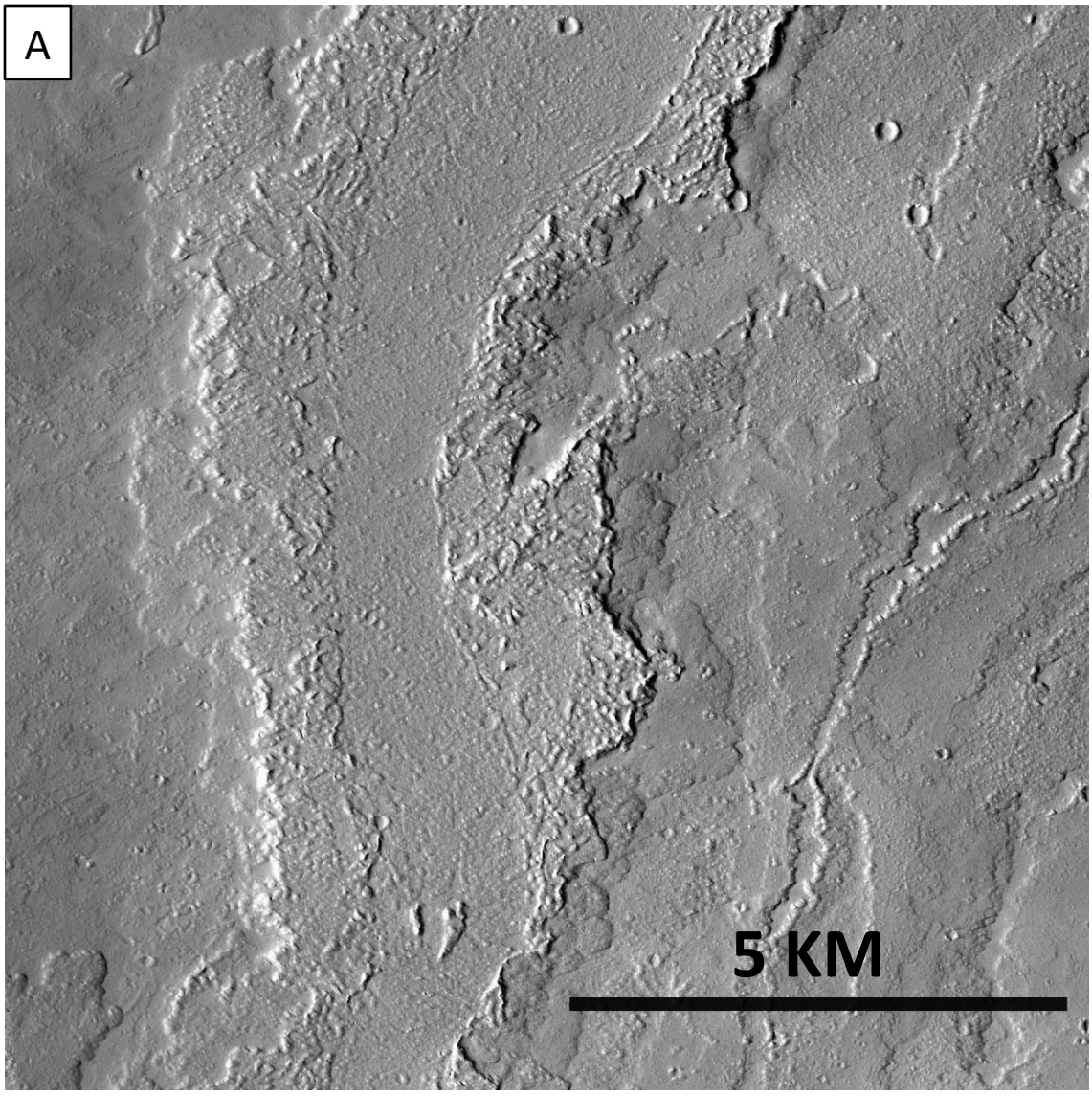

501

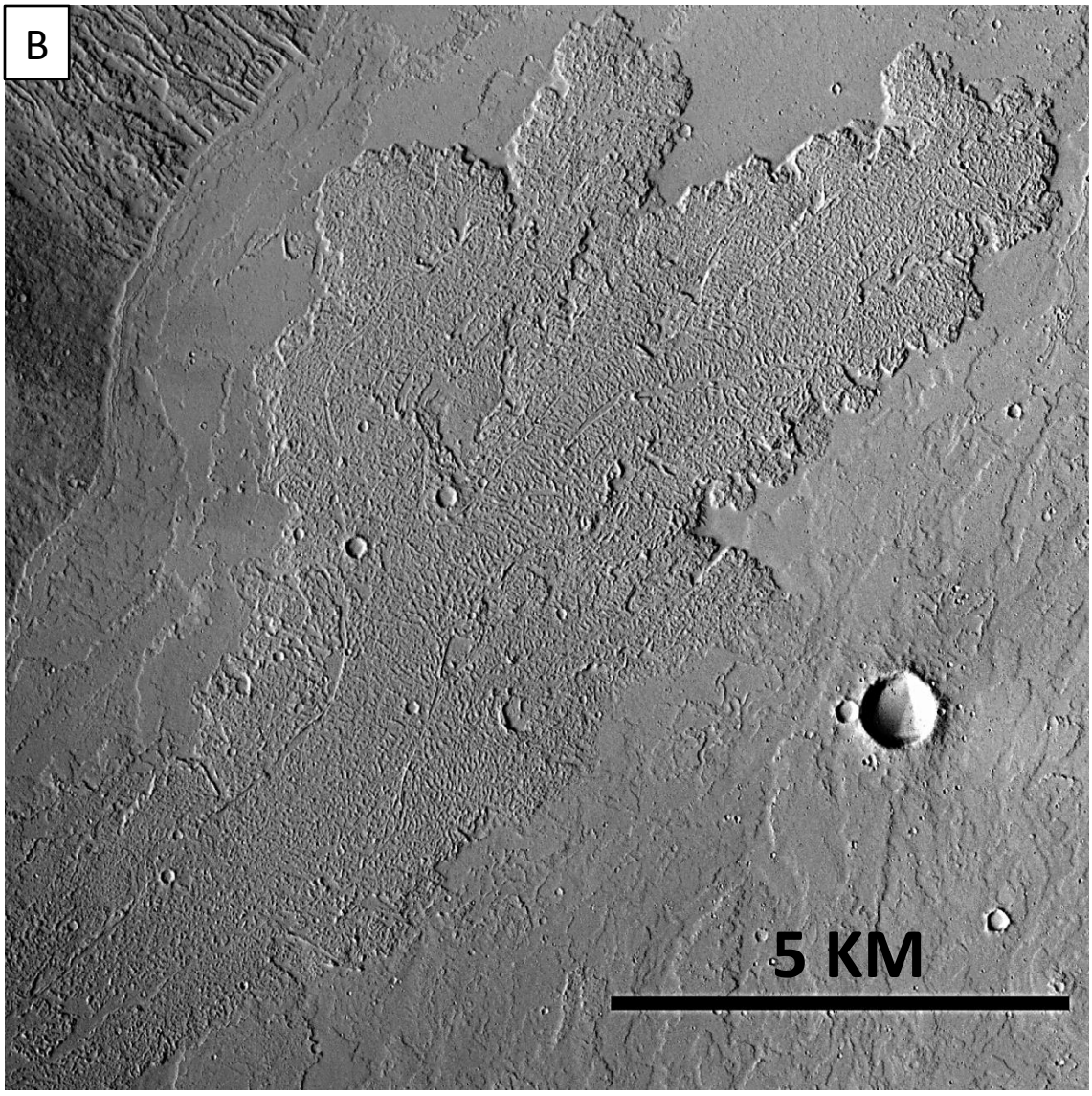
B
5 KM

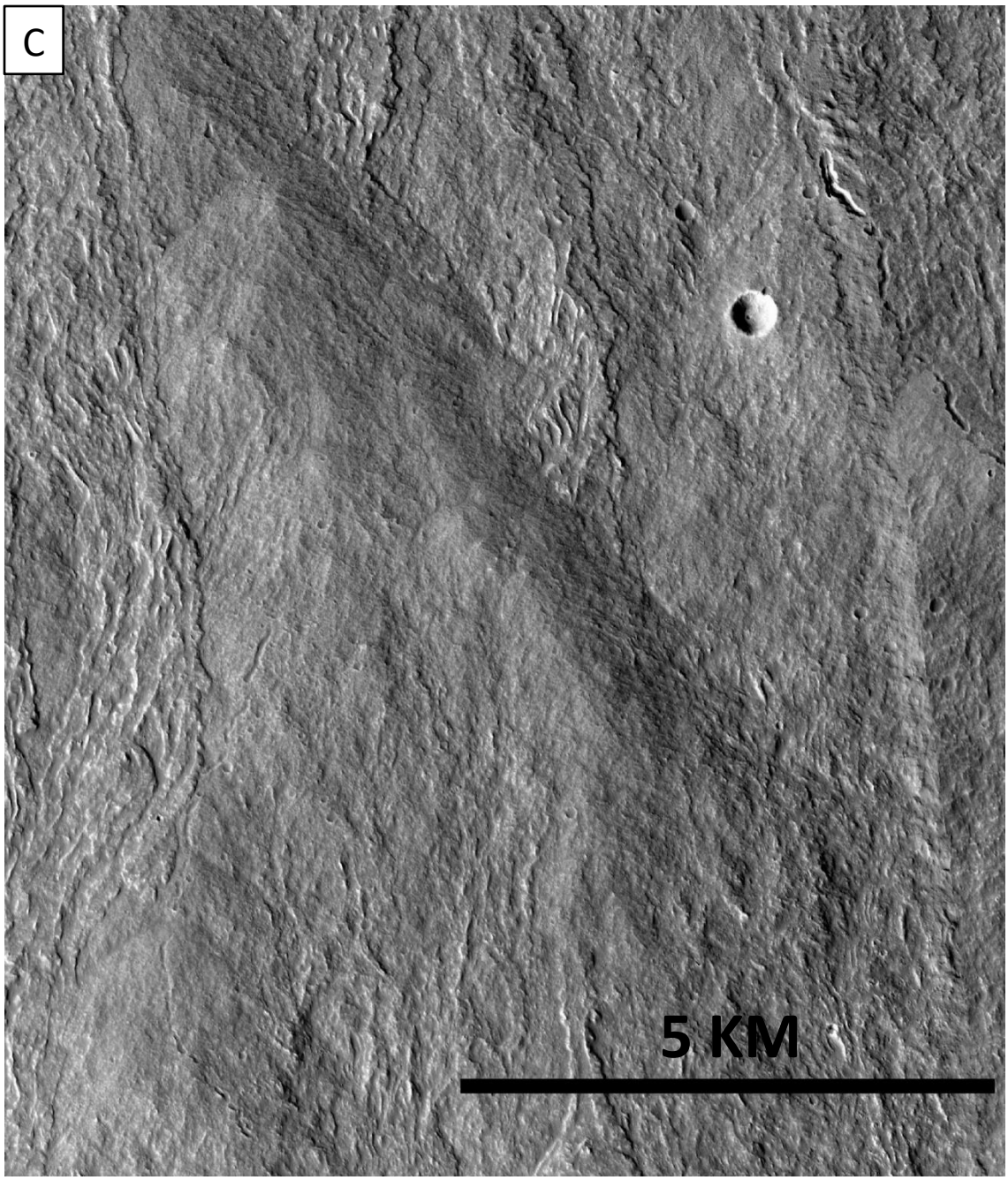

Figure 5: Examples of the three predominant flow morphologies observed in this study. (a) channelized flow (b) corrugated flow (c) ridge flow. North is up in all images. The channelized flow has likely experienced drain out leaving behind a relatively smooth inner channel and raised levees. The ridge flow is likely a channelized flow that has roofed over – a tube-fed flow. Ridge flows are observed on Olympus Mons, Ascraeus Mons, and Alba Mons [*Sakimoto* et al., 1997; *Bleacher* et al., 2007]

5.2. Flow geometries

512 We measured the dimensions – length, width, and thickness – of 40 lava flows in the
513 Tharsis volcanic province on Mars. Using these flow dimensions, we calculated flow volumes.
514 Flows occurred in three subregions: on central volcanoes (i.e. Olympus Mons and Ascraeus
515 Mons apron), in close proximity to central volcanoes (i.e. Olympus Mons and Ascraeus Mons),
516 and in the volcanic plains of Tharsis. The 40 lava flows ranged in length from ~15 to 314 km.
517 The longest flows occurred in the volcanic plains. Mean flow widths ranged from ~0.5 to 29 km,
518 with the narrowest flows occurring on Olympus Mons. Flow thicknesses ranged from ~11 to 91
519 m. Flow areas and volumes ranged from ~14 to 11,180 km^2 and ~1 to 430 km^3, respectively.
520 The smallest flows in areal extent and volume are observed on Olympus Mons and Ascraeus
521 Mons apron, while the largest flows occur in the volcanic plains of Tharsis surrounding the
522 Tharsis Montes and Daedalia Planum. The lava flows were emplaced on slopes ~0.3 – 6.6˚, with
523 the steepest slopes occurring on the flanks of Olympus Mons. Slopes in the volcanic plains
524 typically ranged from ~0.3 to 1˚.

525 5.3. Rheological analyses

526 The methods described above in 4.2.1 were applied to 34 of 40 lava flows. Resulting
527 volumetric flow rates, or effusion rates ranged from 3×10^2 to ~3.5×10^4 m^3/s (Table 2). Higher
528 effusion rates were estimated for the intervolcanic plains and Daedalia Planum, while lower
529 effusion rates were estimated for flows on Olympus Mons. We calculated effective flow
530 viscosities of ~10^4 – 10^7 Pa s and yield strengths of ~800 – 3×10^4 Pa. Viscosities and yield
531 strengths were highest for flows observed on Olympus Mons and lowest for those in the volcanic
532 plains. Modeled emplacement times for the lava flows ranged from 9 days to ~1 year.

533

CALCULATIONS USING GRAETZ NUMBER AND JEFFREY'S EQUATION

FLOW #	Eruption Rate (m^3/s)	Viscosity (Pa-s)	Yield Strength (Pa)
1	1680	9.4×10^4	7.7×10^2
2	16330	2.1×10^6	3.1×10^3
3	34781	9.4×10^5	2.2×10^3
4	60	7.4×10^7	3.1×10^4
5	245	1.4×10^6	1.3×10^4
6	342	3.3×10^7	1.8×10^4
7	3981	7.9×10^5	2.0×10^3
8	2855	1.4×10^5	9.3×10^2
9	2761	1.4×10^6	3.1×10^3
10	3654	2.5×10^6	4.3×10^3
11	3994	6.9×10^6	4.0×10^3
12	17113	4.6×10^6	6.0×10^3
13	11859	9.0×10^5	3.0×10^3
14	5646	1.3×10^6	3.8×10^3
15	3496	1.6×10^5	2.0×10^3
16	4981	1.6×10^5	2.8×10^3
17	4190	2.0×10^5	1.9×10^3
18	656	9.5×10^5	2.0×10^3
19	2145	1.2×10^6	3.5×10^3
20	4816	3.8×10^6	3.3×10^3
21	7881	3.4×10^6	3.4×10^3
22	152	1.1×10^7	1.4×10^4
23			
24	298	7.0×10^6	1.5×10^4
25			
26			
27			
28			
29			
30	1612	3.0×10^6	2.3×10^3
31	255	2.0×10^7	7.5×10^3
32	2255	2.8×10^6	3.4×10^3
33	2151	3.2×10^6	4.1×10^3
34	1585	1.3×10^6	2.8×10^3
35	2875	2.1×10^5	2.2×10^3
36	395	1.6×10^5	1.3×10^3

37	824	2.1×10^5	1.7×10^3
38	5579	1.8×10^5	1.7×10^3
39	3107	7.0×10^5	1.9×10^3
40	8242	9.7×10^6	5.8×10^3

Table 2: Eruption rates and rheological properties of 34 lava flows on Mars using a Graetz number of 300 and Jefferey's equation. Blank cells represent lava ridges, whose eruption rates cannot be estimated based on their morphology.

5.4. Application of Ψ

We used assigned Ψ values to calculate eruption rates and emplacement times for all 40 lava flows. Assuming a solidification temperature of 900˚C and an eruption temperature of 1150˚C, calculated effusion rates using Eqs. 3 and 4 ranged from 0.2 – 6500 m^3/s (Table 3). Effusion rates corresponding to each morphology are: smooth-levee flows (~6500 m^3/s); levee flows (950 – 6500 m^3/s); levee-fold flows (575 – 950 m^3/s); folded flows (35 – 575 m^3/s); rift, or tube-fed, flows (0.2 – 20 m^3/s). The kinematic viscosity was an input instead of an output in this model, and we used a value of ~10^2 Pa s [*Nichols*, 1939; *Hon et al.*, 1994;]. Yield strengths are not an output of Ψ and were not calculated via this method. Emplacement times range from ~14 hours –2200 years. The largest emplacement times (180 – 2200 years) were exclusively for the lava ridge flows and were calculated using the lowest effusion rate of the range – 0.2 m^3/s. If the higher end of the range for lava ridges is used (20 m^3/s), the emplacement times for lava ridges are 1.8 – 22 years. If lava ridges are removed, the emplacement times range from ~14 hours – 9.5 years.

APPLICATION OF Ψ

FLOW #	Eruption Rates (m^3/s)
1	950 - 6500
2	950 - 6500
3	6500
4	575 - 950
5	575 - 950

6	950 - 6500
7	950 - 6500
8	950 - 6500
9	950 - 6500
10	950 - 6500
11	575 - 950
12	950 - 6500
13	950 - 6500
14	950 - 6500
15	575 - 950
16	950 - 6500
17	950 - 6500
18	35 - 575
19	950 - 6500
20	950 - 6500
21	6500
22	950 - 6500
23	0.2 - 20
24	950 - 6500
25	0.2 - 20
26	0.2 - 20
27	0.2 - 20
28	0.2 - 20
29	0.2 - 20
30	950 - 6500
31	950 - 6500
32	950 - 6500
33	950 - 6500
34	950 - 6500
35	950 - 6500
36	950 - 6500
37	950 - 6500
38	950 - 6500
39	950 - 6500
40	950 - 6500

Table 3: Eruption rate ranges for 40 lava flows on Mars by based on surface morphology, assigned Ψ value, and assumed ambient and flow properties.

5.5. Self-replicating lava flow model

The self-replication model as outlined by *Baloga and Glaze* [2008] was applied to 13 qualifying flows to calculate effusion rates and emplacement times as described above.

Viscosities were then calculated by treating the lava as a Newtonian fluid and using Jeffrey's equation (Eq. 2). Yield strengths were calculated by treating the flow as a Bingham fluid (Eq. 4). Modeled effusion rates are ~30 – ~1200 m^3/s (Table 4). Eruption rates were highest for lava flows observed in the volcanic plains. Viscosities ranged from 4.5×10^6 – ~3×10^7 Pa s and yield strengths ranged from ~10^3 Pa – 3.6×10^4 Pa. The time of emplacement for these flows ranges from 4.5 months – 9 years. No appreciable difference in viscosity or emplacement time was observed between the Tharsis subregions.

SELF-REPLICATION LAVA FLOW MODEL [BALOGA & GLAZE, 2008]

FLOW #	Yield Strength (Pa)	Eruption Rate (m^3/s)	Viscosity (Pa-s)
1			
2	3.4×10^3	1174.39	9.5×10^6
3	5.3×10^3	335.62	2.9×10^7
4			
5			
6			
7			
8			
9			
10	4.6×10^3	52.66	3.2×10^7
11			
12			
13			
14	3.3×10^3	135.42	2.0×10^7
15			
16			
17			
18			
19			
20			
21	7.9×10^3	285.09	1.5×10^7
22	1.7×10^4	27.60	2.9×10^7
23			
24	3.6×10^4	26.90	1.5×10^7
25			

26			
27			
28			
29			
30	1.4×10^3	46.00	1.7×10^7
31			
32	2.7×10^3	236.21	1.6×10^7
33	4.0×10^3	204.30	2.2×10^7
34	2.0×10^3	50.57	1.0×10^7
35	2.8×10^3	89.26	2.5×10^6
36			
37			
38			
39	1.4×10^3	111.17	4.5×10^6
40			

Table 4: Eruption rates and rheologic properties of 13 lava flows on Mars using the self-replication model for long lava flows [*Baloga and Glaze*, 2008].

6. Discussion and Implications

6.1. Martian volcanism

6.1.1. Volumes, extent, and distribution of lava flows

Martian volcanism has decreased in spatial extent and frequency. According to a number of studies that have used crater counts, geomorphology, and modelling, the bulk of Martian volcanism occurred >3 Ga during the Noachian and Early Hesperian [e.g. *Plescia*, 2004; *Werner*, 2009; *Tanaka et al.*, 2014]. Early volcanic activity consisted of plains-style volcanism, possible explosive eruptions, and the construction of the large shields [e.g., *Carr*, 1973, 1974; *Plescia*, 2004]. As Mars has cooled over time, the number of volcanoes erupting and the volumes of erupted magma have decreased [e.g., *Greeley and Spudis*, 1981; *Bleacher et al.*, 2007; *Werner*, 2009; *Xiao et al*., 2012]. The flows in our study are among the most recent examples of effusive volcanism in the Tharsis Volcanic Province and on Mars. Studies by *Tanaka et al*. [2014] and *Werner* [2009] suggest that these flows were emplaced in the Late Amazonian and range in age

from 10s – 100s of millions of years old. There is some variability in age among sub-regions within Tharsis. The flows on the flanks of Olympus Mons and Ascraeus Mons are ~100 – 700 Ma and 100 – 800 Ma, respectively, with localized areas < 50 Ma while the aprons emanating from Ascraues Mons aprons are ~1 Ga [e.g., *Neukum et al.*, 2004; *Werner*, 2009], compared to the flows in the volcanic plains that likely range in age from <100 to 400 Ma [e.g. *Hauber et al.*, 2011]. The volumes of eruptions are also less on Olympus Mons and the Ascraues Mons apron relative to the volcanic plains [*Bleacher et al.*, 2007; this study].

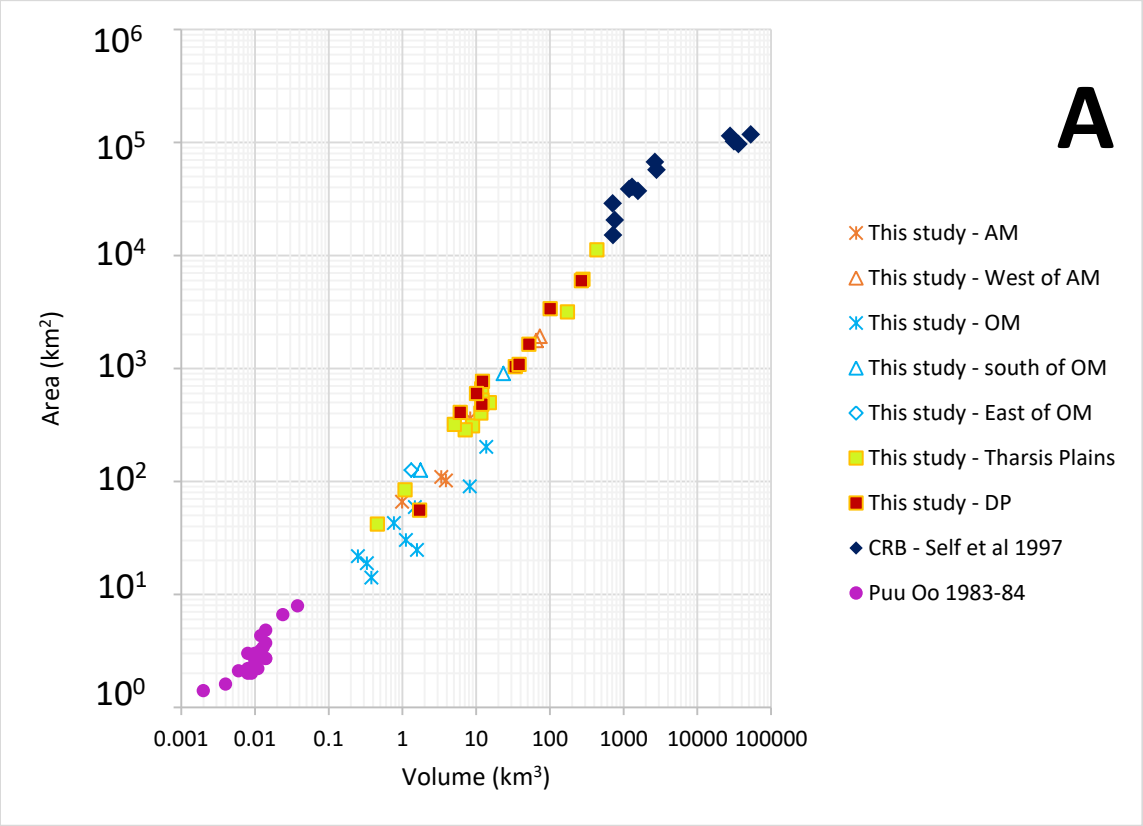

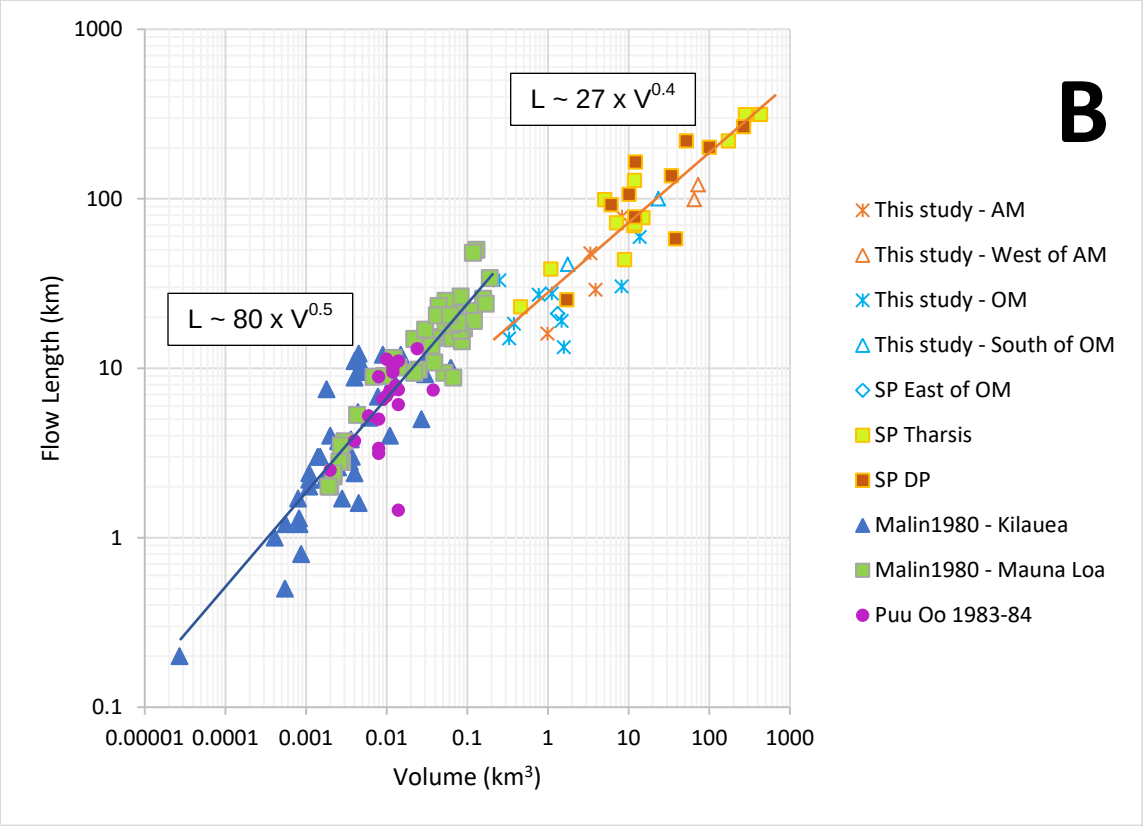

Figure 6: Volumes are expressed as a function of flow length and area covered. AM = Ascraeus Mons; OM = Olympus Mons; DP = Daedalia Planum; CRB = Columbia River Basalts. **(a)** The calculated volumes and area covered of the 40 lava flows observed in this study are plotted along with the 1983-1984 Pu'u O'o lava flows [*Wolf* et al., 1987] and Columbia River Basalt [*Self* et al., 1997]. The smallest flows are not too dissimilar to the Pu'u O'o lava flows, while the largest flows are similar in size and volume to those erupted in the Columbia River basalts. **(b)** Measured flow length is plotted as a function of calculated volume for 40 lava flows on Mars and are compared to terrestrial flows in Hawai'i. The bulk of Martian flows are longer and volumetrically larger, however, a subset of flows primarily related to central volcanoes overlap in length with Mauna Loa flows. Power law relationships (blue line – terrestrial; orange line – Mars) for Hawaiian lava flows are compared to the Martian lava flows. According to *Malin* [1980], an exponent equal to 0.5 indicates both length and cross-sectional area of the flows are controlled by volume. The Mars lava flows have an exponent ~0.4 indicating length and cross-sectional area are largely controlled by volume.

Figure 6a shows the area covered by our flows in km^2 versus their volumes in km^3. In terms of volume and corresponding area, flows on the central volcanoes of Ascreaus Mons (AM) and Olympus Mons (OM) (denoted by stars) are distinct from and smaller than flows associated

608 with plains volcanism (squares). A similar relationship can be seen in Figure 6b where lava flow
609 length (km) is shown against total volume.

610 In Figure 6a, we also compare the Mars flows to well-documented terrestrial flows. We
611 first note that in terms of volume / area, the Mars flows follow the same trend as terrestrial flows
612 and sit directly between Hawaiian flows [Pu'u O'o, 1983-84, *Wolfe et al*., 1987] and flows from
613 the Columbia River Basalts [CRB, *Self et al*., 1996]. Further, the OM and AM flows sit close to
614 the Pu'u O'o flows whereas the plains flows extend over a greater range, reaching but not
615 overlapping with the CRB flows. We also note that the plains flows are longer than flows
616 erupted from central vents (Fig. 6b).

617 In Figure 6b, we note that the relationship between volume and length follows a power
618 law for both terrestrial and Mars flows. The terrestrial flows follow a relationship with a power-
619 law exponent of roughly 0.5. According to *Malin* [1980] a power-law exponent of 0.33 would
620 indicate that flow length, width, and depth are equally controlled by (and proportional to) the
621 volume erupted, whereas an exponent of 1 would indicate that the cross-sectional area of the
622 flow does not vary with volume, and thus only the length is controlled by volume. *Malin* [1980]
623 interprets the exponent of 0.5 to indicate that both the length and cross-sectional area (product of
624 thickness and width) of the flows are controlled by the volume, and that length and cross-
625 sectional area are mutually dependent. The Mars flows can be fitted by an exponent close to 0.4,
626 again suggesting that volume controls both length and cross-sectional area, with the <0.5
627 exponent of the Mars flows possibly reflecting their wide range of substrate slopes and
628 viscosities that also control flow geometry in complex ways.

629 6.1.2 Model Results: effusion rate, duration, and rheology

630 Our calculated effusion rates allow differentiation among the subregions (Figure 7a), with
631 the highest rates estimated for the plains regions (squares) and the lowest values estimated for
632 Ascreaus and Olympus Mons (stars). Regions located between central volcanoes and volcanic
633 plains (triangles) have intermediate effusion rates. The application of the halting Graetz number
634 (G_z = 300) and the self-replicating model of *Glaze and Baloga* [2008] produce eruption rates for
635 Ascreaus and Olympus Mons that match well to terrestrial values despite the much greater
636 volumes of the Mars flows (Fig. 7b, c, orange vs. purple Xs). Eruption rates for the plains
637 regions on Mars exceed many Hawaiian eruption rates but are consistent with some of the
638 highest eruption rates measured at the Pu'u O'o vent [1983-84, *Wolfe et al*., 1987] and Mauna
639 Loa [1984, *Lipman and Banks*, 1987]. Lower eruption rates are estimated when flow
640 morphology and mass allocation to levees are taken into account in the self-replicating model
641 [Fig. 7; *Glaze and Baloga*, 2006; *Baloga and Glaze*, 2008]. Eruption rates obtained using Ψ
642 morphologies span nearly the entire range of available terrestrial values and those obtained by
643 the two other models, with the exception of the uppermost values calculated by assuming a
644 halting G_z = 300.

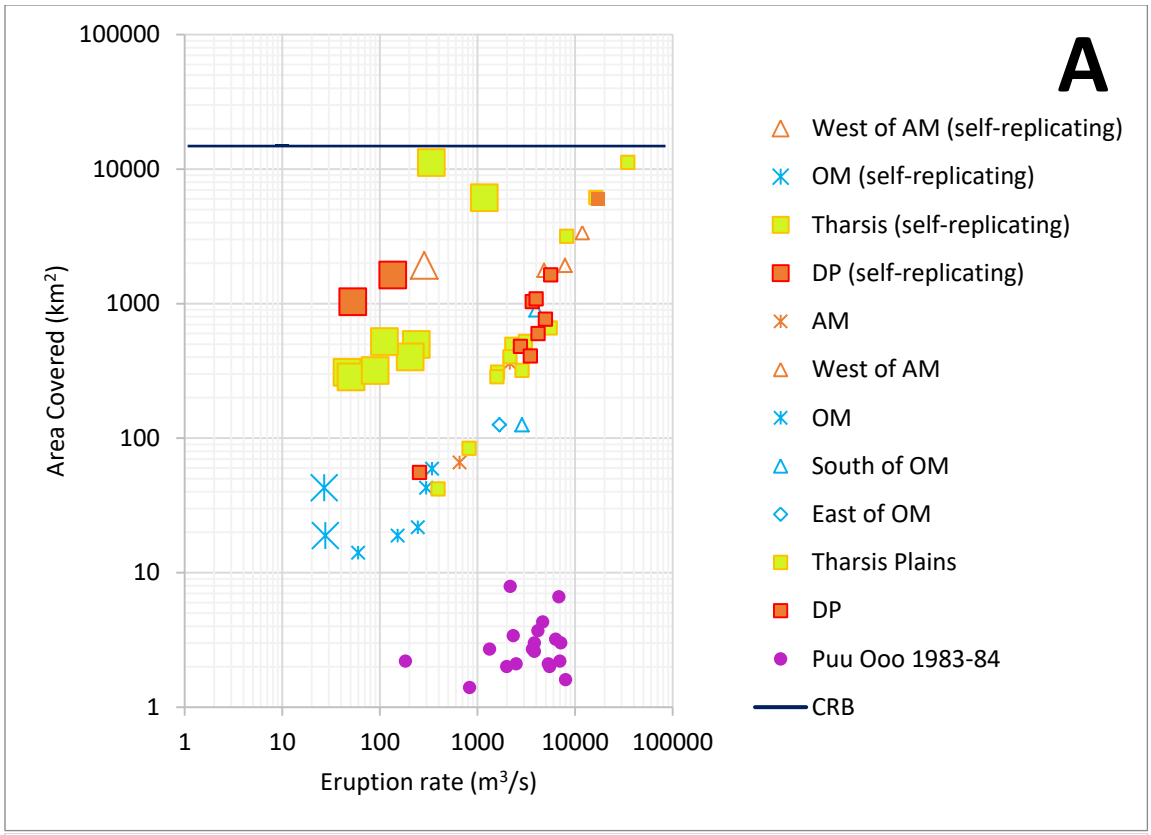
A
100000
10000
1000
100
10
1
Area Covered (km²)
1
10
100
1000
10000
100000
Eruption rate (m³/s)
West of AM (self-replicating)
OM (self-replicating)
Tharsis (self-replicating)
DP (self-replicating)
AM
West of AM
OM
South of OM
East of OM
Tharsis Plains
DP
Puu Ooo 1983-84
CRB

645

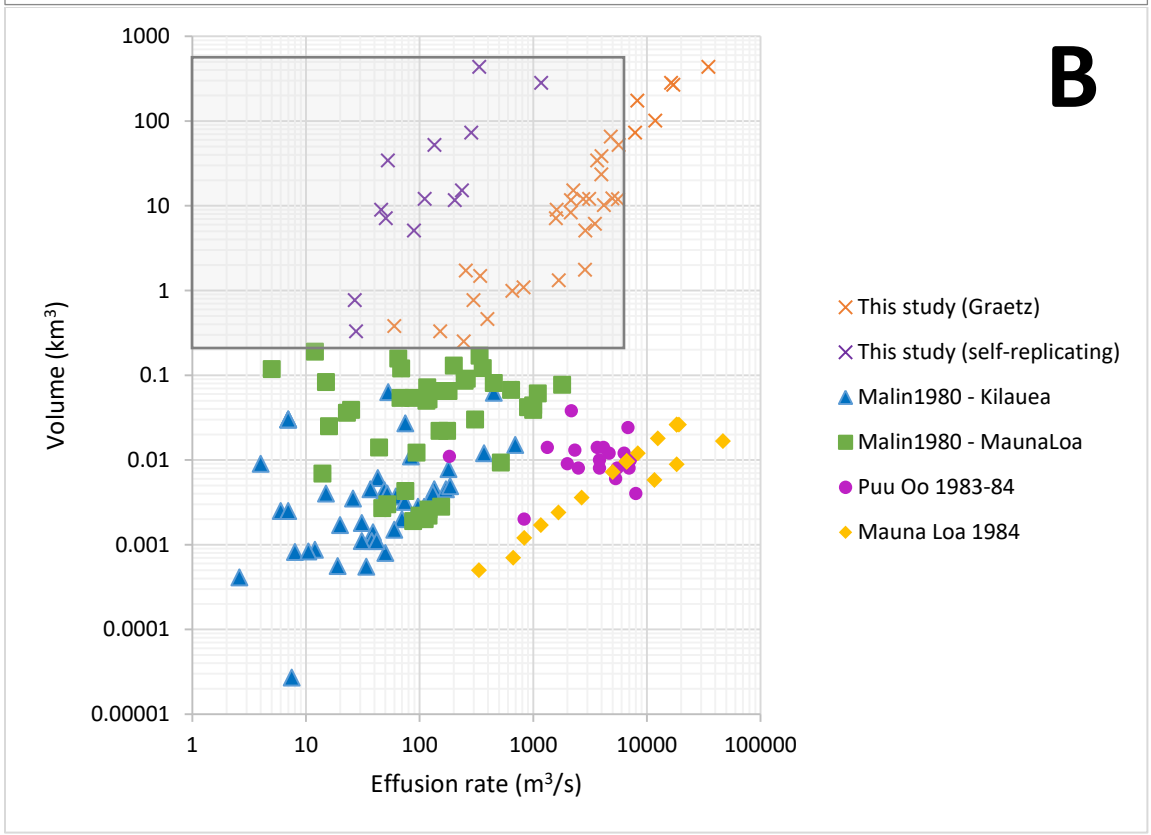
B
1000
100
10
1
0.1
0.01
0.001
0.0001
0.00001
Volume (km³)
1
10
100
1000
10000
100000
Effusion rate (m³/s)
This study (Graetz)
This study (self-replicating)
Malin1980 - Kilauea
Malin1980 - MaunaLoa
Puu Oo 1983-84
Mauna Loa 1984

646

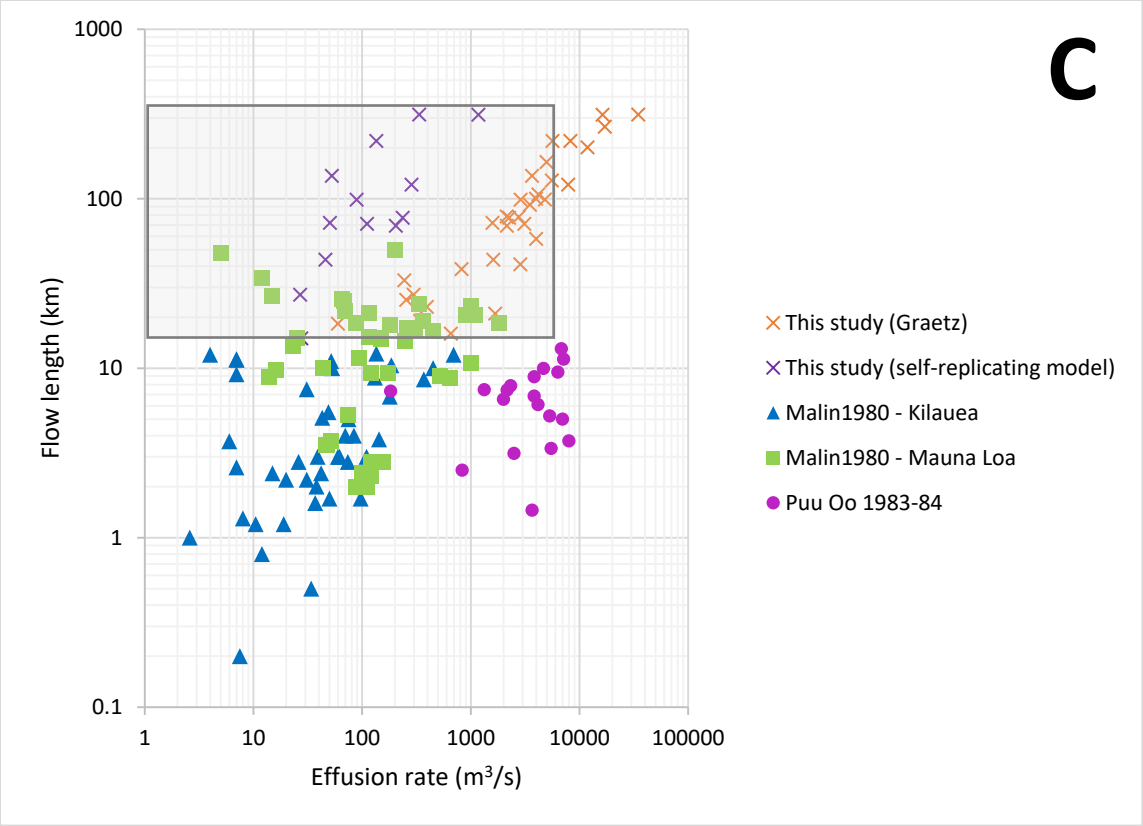

Figure 7: AM = Ascraeus Mons; OM = Olympus Mons; DP = Daedalia Planum. **(a)** Relationship between eruption rate and area covered. The Mars flows are compared to flows erupted during the 1983-84 Pu'u O'o eruption in Hawai'i and the Columbia River Basalts (CRB). Large symbols denote values derived using self-replication model for long lava flows. Small symbols indicate values calculated using Graetz number. Stars indicate values obtained for central volcanoes. Navy blue line denotes minimum areal extent of CRB flows from *Self et al.* [1997]. This data supports the conclusion that eruption rates are controlled by subregions, with higher eruption rates calculated for the volcanic plains than central volcanoes. In general, the self-replication model produces lower eruption rates than using the Graetz number. **(b)** The relationship between eruption rate and total erupted volume. The eruption rates for the Mars lava flows are comparable to terrestrial values. The highest eruption rates calculated for Mars are similar to the highest values observed on Earth during the Mauna Loa eruption of 1984. Although the lower volume estimates are similar to those observed on Mauna Loa, most of the flow volumes are 2 – 4 orders of magnitude greater. **(c)** Figured modified from *Walker* [1973]. Log-log plot shows the length of lava flows as function of the eruption rate for terrestrial lava flows at Mauna Loa and Kilauea. Superposed on that figure are the eruption rates calculated using the three models in this study. Orange X's are calculated eruption rates using Graetz number. Purple X's are eruption rates calculated from self-replication model. Shaded gray box represents ranges of eruption rates calculated using Ψ.

The flows on Olympus Mons are smaller than those observed in the volcanic plains of Tharsis and tend to be open channel flows, which may suggest short-lived, volume-limited

eruptions [*Bleacher et al.*, 2007]. The flows in the volcanic plains are larger in areal extent than flows observed on Olympus Mons or the Ascraeus Mons apron. The variability in flow volume by subregion suggests different eruption conditions, specifically differences in subsurface pathways and magma sources. The volumetrically larger flows were likely erupted to the surface by large dikes and remained active for long periods of time (Fig. 8), consistent with findings of *Wilson and Head* [1983]. Meanwhile, the flows on Olympus Mons and proximal to Ascraeus Mons were likely emplaced by smaller subsurface conduits that were active for shorter periods of time consistent with findings of *Bleacher et al.* [2007] and *Wilson and Head* [1983]. We also note that the largest of the Mars flows, given the measured volumes and calculated eruption rates, must have been active much longer than typical terrestrial flows from places like Hawaii (Fig. 8), but may rather be akin to regions like the Columbia River Basalts which are thought to have been active over long periods to generate voluminous fields; this is particularly likely for the Mars plains volcanism characterized here [*Self et al*., 1996].

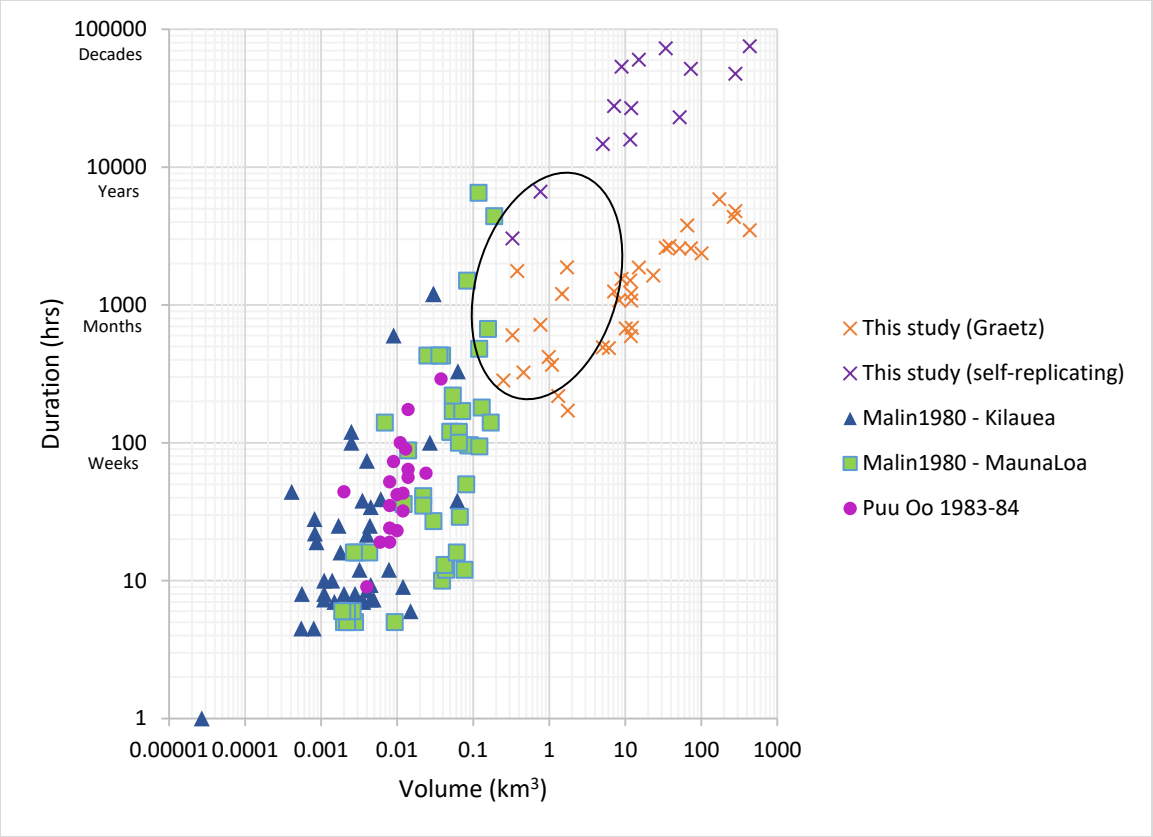

Figure 8: The calculated volume of Mars lava flows is compared to terrestrial flows as a function of duration of emplacement. Black circle contains Mars flows associated with central volcanoes, whereas remaining flows were produced in the plains. The Mars lava flows are much larger in volume – although some values are similar to Mauna Loa – and erupted over greater lengths of time. This suggests that feeder dikes and other pathways necessary to producing these flows remained active and open for longer periods than pathways on Earth.

6.1.3 Comparison to previous work

Our results are generally consistent with other studies: *Hiesinger et al.* [2007] calculated effusion rates for 25 young flows on the eastern flank of Ascraeus Mons, resulting in a range of ~20 to ~400 m^3/s that falls within the range we calculated for nearby flows using all three models. On the other hand, our effusion rates for the lava ridges, interpreted as tube-fed flows (0.2 – 20 m^3/s) fall at the very low end of the range proposed by *Sakimoto et al.* [1997] of 2 – 10^5 m^3/s. Despite the long runouts of lava flows in the Tharsis region of Mars, our analysis shows that very high effusion rates of ~10^5 m^3/s are not required to explain the observed flows.

699 Earlier studies of Martian volcanism invoked ultramafic and other exotic compositions to
700 explain the large, voluminous effusive eruptions preserved across the surface of the planet [e.g.,
701 *Sakimoto et al.*, 1997; *Cashman et al.*, 1998; *Garry et al.*, 2007]. While the ranges differ
702 depending on the model, the viscosities of $10^4 – 10^7$ Pa s calculated in this study are consistent
703 with a basalt to basaltic andesite composition, which is observed on all dust-free Martian
704 surfaces [*Rogers and Christensen*, 2007]. These viscosities are similar to those calculated for the
705 25 young lava flows observed (10^4-10^7 Pa-s) by *Hiesinger* et al. [2007] and the 8 lava flows
706 observed in the volcanic plains of Tharsis (10^2-10^3 Pa-s) by *Hauber* et al. [2011]. In Hawaii,
707 recently erupted basalt has viscosities ~$10^2 – 10^3$ Pa s, similar to Mt. Etna (~10^3) [e.g., *Self et al.*,
708 2008; *Harris and Rowland*, 2015]. The viscosity of some Columbia River Basalt and Deccan
709 Trap lavas has been estimated to be 500 and 100 Pa s at the time of emplacement [e.g., *Self et al.*,
710 1997; 2008].
711 The rheologic model results in slightly lower calculated viscosities, due to the estimate of
712 effusion rate (Q) which could be an order of magnitude higher than reality because it assumes the
713 entire flow front is active during the time of emplacement. Jeffrey's equation is particularly
714 sensitive to the flow thickness. The flow thicknesses measured in our study are taken to be the
715 maximum thickness, assuming erosion and gradation has not significantly altered the flow. The
716 self-replication model produces viscosity values at the higher end of basalt ($10^6 – 10^7$ Pa s) and
717 more congruent with basaltic andesite or a highly crystallized basalt. *Baloga and Glaze* [2008]
718 obtained a value of 10^6 Pa-s for one very long lava flow which is the same flow as our Flow 2,
719 for which we calculated ~10^7 Pa-s. The difference is due to differing flow lengths: *Baloga and*
720 *Glaze* [2008] measured a 173 km flow length, whereas we measured 313 km for the same flow.
721 6.1.4 Planetary evolution & interior

Martian volcanism, although widespread early in its history, has become more localized with time. The most recent episodes of volcanism have occurred near the Elysium Mons volcanic province around Cerberus Fossae and the Tharsis Volcanic Province [e.g., *Neukum et al.*, 2004; *Werner*, 2009], with both provinces separated by thousands of kilometers. The effusion rates and viscosities of the most recent eruptions studied here (~10s – 100s Ma likely in the plains, Figs. 8 and 9) suggests that Martian interior has produced eruptions on par with those of flood basalts and large igneous provinces on Earth. Our modeled durations (Fig. 9) imply that a large supply of eruptible magma had an open pathway to the surface over long periods of time, particularly in the volcanic plains [e.g. *Wilson and Head*, 1983]. Given the volumes calculated in this study, these pathways would have been linked to sizeable magma bodies. The observation of relatively young low shields in the volcanic plains of Tharsis (<100 Ma) might hint at a larger magma body, perhaps related to the proposed plume beneath Tharsis [e.g., *Dohm et al.*, 2017].

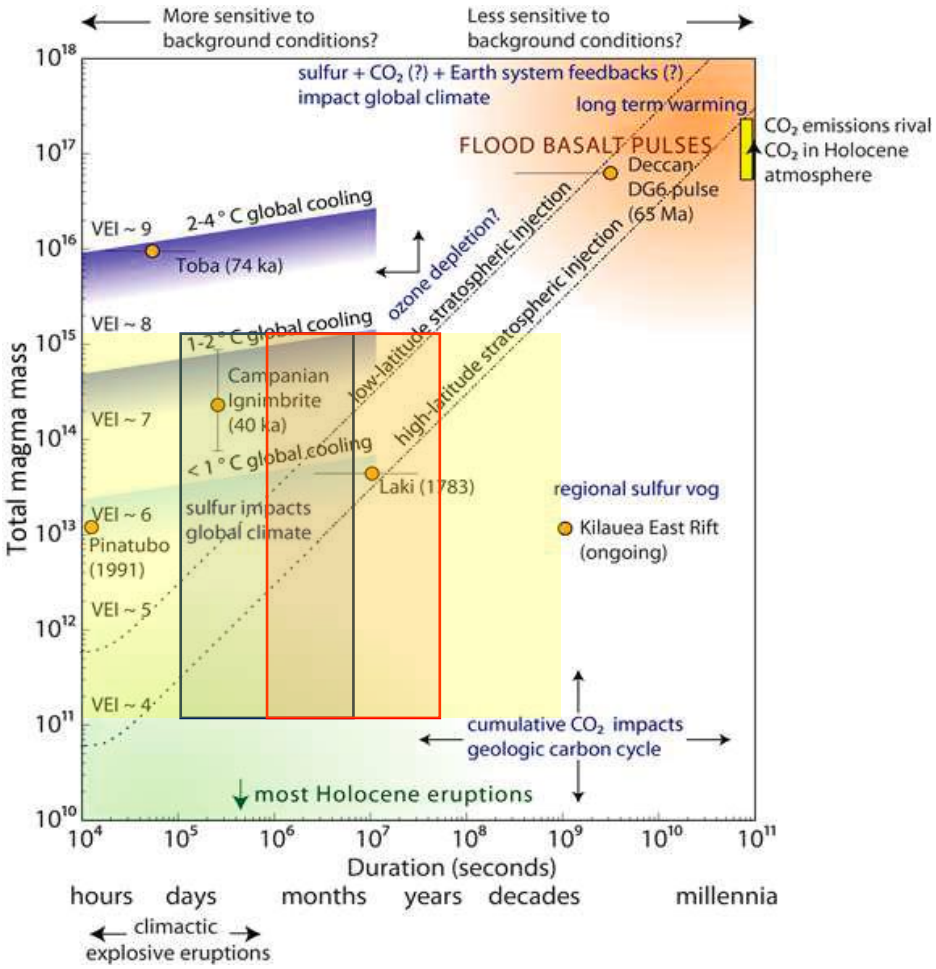

Figure 9: Mass of martian flows and emplacement times are compared with notable terrestrial eruptions. Blue box represents Graetz number minimum eruption durations, while red box represents self-replication model eruption durations. Green box represents eruption durations for full range of Ψ derived eruption rates. Modified from Black and Manga [2017].

The contribution of effusive volcanism to climate has been a subject of open speculation for terrestrial and extraterrestrial systems, such that both total mass erupted and eruption duration play a role in controlling climate forcing [Figure 9; *Self et al.*, 1997; *Black and Manga*, 2017; *Rader et al.*, 2017]. Some of the eruptions represented by the lava flows in our study may have lasted for decades and the masses are on the order of very large terrestrial eruptions. The masses of individual flows calculated in our study are less than that of complete members in terrestrial large igneous provinces, but some, especially those in the plains, do overlap with other eruptions that had significant global impacts, consistent with up to 2 degrees of global cooling. While

large igneous provinces typically erupt over millions of years on Earth, the Tharsis volcanic province has produced volcanic eruptions over billions of years [e.g., *Self et al.*, 1996; 1997; 2008; *Sheth*, 2006; *Werner*, 2009; *Tanaka et al.*, 2014], possibly enhancing their capacity for atmospheric forcing. And, the high altitude of the eruptions at Tharsis may have further enhanced their ability to produce climatic impacts [e.g., *Sheth*, 2006]. Whether or not those eruptions were continuous or volumetrically significant enough to impact the atmosphere remains an open question, although our analysis demonstrates that individual flows in Tharsis are at the very least of the scale of large terrestrial eruptions that caused short term changes to global climate.

7. Conclusions

This study produced volumes, effusion rates, viscosities, and emplacement times for 40 lava flows in the Tharsis Volcanic Province on Mars. The results have implications for recent volcanism on Mars, lava composition, the plumbing of the Martian subsurface, and potential climatic effects. Sub-regional differences in flow volumes across the Tharsis volcanic province suggest different magma sources and subsurface plumbing conditions for central volcanoes and lava plains. Drawing from these analyses, we conclude the following:

1. Martian lava flows do not require extremely high volumetric flow rates or exotic lava compositions. Observed lava flows can be produced by terrestrial volumetric flow rates and non-exotic lava compositions with viscosities and yield strengths suggestive of basalt and basaltic andesite compositions.
2. Subsurface pathways in the Martian interior were long-lived and capable of erupting melts for months to years in some cases producing individual lava flows of remarkable length and volume. Additionally, if the ages of the flows are accurate,

magma was being stored and transported throughout the Martian crust from the mantle within the last 1 Ga – and as recent as ~10 – 100 Ma during the Late Amazonian.

3. Olympus Mons has produced volumetrically smaller recent eruptions than sources of lava flows in the volcanic plains, suggesting smaller dikes and possibly a smaller, secondary magma source within Olympus Mons. The volcanic plains may be fed directly through a thinner overlying crust by a more abundant source related to a mantle plume or a young plume head.
4. Given the volume of some erupted flows, it is possible that the corresponding volcanic activity impacted the Martian climate, but whether or not those impacts were regional or global, short-term or long-term is unknown.

Acknowledgements

This work was supported by a NASA / JPL THEMIS contract 1228404. NASA spacecraft data used in this study are referred to in the Methods section of this paper. Data generated in this work and used in the figures can be found in a supporting Excel file and will be made available in the appropriate data repository after review.

8. References

Baloga, S.M., and L.S. Glaze (2008), A self-replication model for long channelized lava flows on the Mars plains, *J. Geophys. Res.*, 113, E05003, doi: 10.1029/2007JE002954.

Baloga, S.M., Glaze, L.S., Crisp, J.A., and S.A. Stockman (1998), New statistics for estimating the bulk rheology of active lava flows: Puu Oo examples, *J. Geophys. Res.*, 103, No. B3, 5133–5142.

Black, B.A., and M. Manga (2016), The eruptibility of magmas at Tharsis and Syrtis Major on Mars, *J. Geophys. Res. Planets*, 121, 944–964, doi: 10.1002/2016JE004998.

Black, B.A., and M. Manga (2017), Volatiles and the tempo of flood basalt magmatism, *Earth Planet. Sci. Lett.*, 458, 130–140.

Bleacher, J.E., Greeley, R., Williams, D.A., Werner, S.C., Hauber, E., and G. Neukum (2007), Olympus Mons, Mars: Inferred changes in late Amazonian aged effusive activity from lava flow mapping of Mars Express High-Resolution Stereo data, *J. Geophys. Res., 112*, E04003, doi: 10.1029/2006JE002826.

Bleacher, J.E., Greeley, R., Williams, D.A., Cave, S.R., and G. Neukum (2007), Trends in effusive style at the Tharsis Montes, Mars, and implications for the development of the Tharsis province, *J. Geophys. Res.*, 112, E09005, doi: 10.1029/2006JE002873.

Bleacher, J.E., Orr, T.R., de Wet, A.P., Zimbelman, J.R., Hamilton, C.W., Garry, W.B., Crumpler, L.S., and D.A. Williams (2017), Plateaus and sinuous ridges as the fingerprints of lava flow inflation in the Eastern Tharsis Plains of Mars, *J. Volcano. Geotherm. Res.*, http://dx.doi.org/10.1016/j.jvolgeores.2017.03.025.

Bruno, B.C., Baloga, S.M., and G. J. Taylor (1996), Modeling gravity-driven flows on an inclined plane, *J. Geophys. Res.*, 101, No. B5, 11,595–11,577.

Byrne, P.K., B. van Wyk de Vries, J.B. Murray, V.R. Troll (2012), A volcanotectonic survey of Ascraeus Mons, Mars, *J. Geophys. Res., 117,* E01004, doi: 10.1029/2011JE003825.

Carr, M.H. (1973), Volcanism on Mars, *J. Geophys. Res.*, *78*, 4049 – 4062.

Carr, M.H. (1974), Tectonism and Volcanism of the Tharsis Region of Mars, *J. Geophys. Res.*, *79, no. 26,* 3942 – 3949.

Cashman, K., Pinkerton, H., and J. Stephenson (1998), Introduction to special section: Long lava flows, *J. Geophys. Res.*, 103, no. B11, 27,281–27,289.

Chemical Rubber Company (CRC) (1984), CRC Handbook of Chemistry and Physics. Weast, Robert C., editor. 65th edition. *CRC Press, Inc*. Boca Raton, Florida. USA.

Christensen, P.R. (1986), Regional Dust Deposits on Mars: Physical Properties, Age, and History, *J. Geophys. Res., 91, no. B3,* 3533 – 3545.

Christensen, P.R., B.M. Jakosky, H.H. Kieffer, M.C. Malin, H.Y. McSween, K. Nealson, G.L. Mehall, S.H. Silverman, S. Ferry, M. Caplinger, and M. Ravine (2004), The Thermal Emission Imaging System (THEMIS) for the Mars 2001 Odyssey Mission, *Space Sci. Rev., 110,* 85 – 130.

Crane Company (1988), Flow of fluids through valves, fittings, and pipe, *Technical Paper No. 410* (TP 410).

Crown, D.A., and M.S. Ramsey (2016), Morphologic and thermophysical characteristics of lava flows southwest of Arsia Mons, Mars, *J. Volcanol. Geotherm. Res.*, http://dx.doi.org/10.1016/j.volgeores.2016.07.008.

Crumpler, L.S., and J.C. Aubele (1978), Structural Evolution of Arsia Mons, Pavonis Mons, and Ascraeus Mons: Tharsis Region of Mars, *Icarus*, 34, 496–511.

835 Dohm, J.M., Baker, V.R., Maruyama, S., and R.C. Anderson (2007), Traits and Evolution of the
836 Tharsis superplume, Mars, *Superplumes: Beyond Plate Tectonics*, 523 – 536.
837 Fink, J.H., Park, S.O., and R. Greeley (1983), Cooling and deformation of sulfur flows, *Icarus*,
838 56, 38–50.
839 Fink, J.H., and R. W. Griffiths (1990), Radial spreading of viscous-gravity currents with
840 solidifying crust, *J. Fluid Mech.*, 221, 485–509.
841 Garry, W.B., Zimbelman, J.R., and T.K.P. Gregg (2007), Morphology and emplacement of a
842 long-channeled lava flow near Ascraeus Mons volcano, Mars, *J. Geophys. Res.*, 112,
843 E08007, doi: 10.1029/2006JE002803.
844 Giacomini, L., Massironi, M., Martellato, E., Pasquare, G., Frigeri, A., and G. Cremonese
845 (2009), Inflated flows on Daedalia Planum (Mars)? Clues from a comparative analysis with
846 the Payen volcanic complex (Argentina), *Planet. Space Sci.*, 57, 556–570.
847 Giacomini, L., Carli, C., Sgavetti, M., and M. Massironi (2012), Spectral analysis and geological
848 mapping of the Daedalia Planum lava field (Mars) using OMEGA data, *Icarus*, 220, 679 –
849 693.
850 Glaze, L.S., and S.M. Baloga (2006), Rheologic inferences from the levees of lava flows on
851 Mars, *J. Geophys. Res.*, 111, E09006, doi: 10.1029/2005JE002585.
852 Glaze, L.S., Baloga, S.M., Garry, W.B., Fagents, S.A., and C. Parchetta (2009), A hybrid model
853 for leveed lava flows: Implications for eruption styles on Mars, *J. Geophys. Res.*, 114,
854 E07001, doi: 10.1029/2008JE003278.
855 Gorelick, N.S., Weiss-Malik, M., Steinber, B., and S. Anwar (2003), JMARS: A Multimission
856 Data Fusion Applciation, *34th Lunar and Planetary Science Conference*, abstract no. 2057.

857 Gregg, T.K.P., and J. H. Fink (1996), Quantification of extraterrestrial lava flow effusion rates
858 through laboratory simulations, *J. Geophys. Res.*, 101, No. E7, pp. 16891–16900,
859 96JE01254.
860 Gregg, T.K.P., and J. H. Fink (2000), A laboratory investigation into the effects of slope on lava
861 flow morphology, *J. Volcano. and Geotherm. Res.*, 96, 145–159.
862 Greeley, R., and P.D. Spudis (1981), Volcanism on Mars, *Rev. Geophys. Spac. Phys.*, 19, no. 1,
863 13 – 41.
864 Griffiths, R.W. and J.H. Fink (1992), The morphology of lava flows in planetary environments:
865 predictions from analog experiments, *J. Geophys. Res. Solid Earth*, 97, B13, 19739–19748.
866 Guest, J.E., Kilburn, CRJ, Pinkerton, H., and A.M. Duncan (1987), The evolution of lava flow-
867 fields: observations of the 1981 and 1983 eruptions of Mount Etna, Sicily, *Bull Volcanol*, 49,
868 527–540.
869 Harris, A.J.L., and S.K. Rowland (2015), Lava flows and rheology, *The Encyclopedia of*
870 *Volcanoes 2nd Edition*, 321 – 342.
871 Hauber, E., Broz, P., Jagert, F., Jodlowski, P., and T. Platz (2011), Very recent and wide-spread
872 basaltic volcanism on Mars, *Geophys. Res. Lett.*, 38, L10201, doi: 10.1029/2011GL047310.
873 Hiesinger, H., Head III, J.W., and G. Neukum (2007), Young lava flows on the eastern flank of
874 Ascraeus Mons: Rheological properties derived from High Resolution Stereo Camera
875 (HRSC) images and Mars Orbiter Laser Altimeter (MOLA) data, *J. Geophys. Res.*, 112,
876 E05011, doi: 10.1029/2006JE002717.
877 Hon. K., Kauahikaua, J., Denliger, R., and K. Mackay (1994), Emplacmenet and inflation of
878 pahoehoe sheet flows: observations and measurements of active lava flows of Kilauea
879 volcano, Hawaii, *Geologic. Soc. Amer. Bull.*, 106, 351–370.

880 Hulme, G. (1974), The interpretation of lava flow morphology, *Geophys. J. R. astr. Soc.*, 39, 361
881 – 383.
882 Hulme, G. (1976), The Determination of the Rheological Properties and Effusion Rate of an
883 Olympus Mons Lava, *Icarus, 27*, 207 – 213.
884 Hulme, G., and G. Fielder (1977), Effusion rates and rheology of lunar lavas, *Phil. Trans. R. Soc.*
885 *Lond.* A., 285, 227 – 234.
886 Jaumann, R., G. Neukum, T. Behnke, T.C. Duxbury, K. Eichentopf, J. Flohrer., S. Van Gasselt,
887 B. Giese, K. Gwinner, E. Hauber, H. Hoffmann, A. Hoffmeister, U. Köhler, K.-D. Martz,
888 T.B. McCord, V. Mertens, J. Oberst, R. Pischel, D. Reiss, E. Ress, T. Roatsch, P. Saiger, F.
889 Scholten, G. Schwartz, K. Stephan, M. Wählisch and The HRSC Co-Investigator Team
890 (2007), The high-resolution stereo camera (HRSC) experiment on Mars Express: instrument
891 aspects and experiment conduct from interplanetary cruise through the nominal mission,
892 *Planet. Space Sci., 55*, 928 – 952.
893 Jeffreys, H. (1925), The flow of water in an inclined channel of rectangular section, *The London,*
894 *Ediburgh, and Dublin Phil. Mag. J. Sci.*, 49:293, 793 – 807, doi:
895 10.1080/14786442508634662.
896 Lipman, P.W., and N.G. Banks (1987), AA Flow dynamics, Mauna Loa, *Volcanism in Hawai'i*,
897 1527 – 1567.
898 Malin, M.C., J.F. Bell, B.A. Cantor, M.A. Caplinger, W.M. Calvin, R.T. Clancy, K.S. Edgett, L.
899 Edwards, R.M. Haberle, P.B. James, S.W. Lee, M.A. Ravine, P.C. Thomas, and M.J. Wolff
900 (2007), Context camera investigation on board the Mars Reconnaissance Orbiter, *J. Geophys.*
901 *Res., 112*, E05S04, doi: 10.1029/2006JE002808.

McEwan, A.S., E.M. Eliason, J.W. Bergstrom, N.T. Bridges, C.J. Hansen, W.A. Delamere, J.A. Grant, V.C. Gulick, K.E. Herkenhoff, L. Keszthelyi, R.L. Kirk, M.T. Mellon, S.W. Squyres, N. Thomas, and C.M. Weitz (2007), Mars Reconnaissance Orbiter's High-Resolution Imaging Science Experiment (HiRISE), *J. Geophys. Res.*, *112*, E05S02, doi:10.1029/2005JE002605.

Mellon, M.T., Jakosky, B.M., Kieffer, H.H., and P.R. Christensen (2000), High-resolution thermal inertia mapping from the Mars Global Surveyor Thermal Emission Spectrometer, *Icarus*, 148, 437 – 455, doi: 10.1006/icar.2000.6503.

Moore, H.J., Arthur, D.W.G., Schaber, G.G. (1978), Yield strengths of flows on the Earth, Mars, and Moon, *Proc. Lunar Planet. Sci. Conf. 9th*, 3351 – 3378.

Nichols, R. L. (1939), Viscosity of Lava, *J. Geology*, 47, no. 3, 290 – 302.

Neukum, G., R. Jaumann., H. Hoffmann, H., E. Hauber, J.W. Head, A.T. Basilevsky, B.A. Ivanov, S.C. Werner, S. van Gasselt, J.B. Murray, T. McCord, and The HRSC Co-Investigator Team (2004), Recent and episodic volcanic and glacial activity on Mars revealed by the High-Resolution Stereo Camera, *Nature*, 432, 971 – 979.

Pasckert, J. H., Hiesinger, H., and D. Reiss (2012), Rheologies and ages of lava flows on Elysium Mons, Mars, *Icarus*, 219, 443 – 457.

Peck, D.L. (1978), Cooling and Vesiculation of Alae Lava Lake, Hawai'i, *Geologic. Surv. Pro. Paper*, 935-B.

Peters, S.I. (2020), Investigating Lava Flow Emplacement: Implications for Volcanic Hazards and Planetary Evolution, *Arizona State University*, *ProQuest Dissertations Publishing*, thesis.

924 Peters, S.I., and P.R. Christensen (2017), Flank vents and graben as indicators of Late
925 Amazonian volcanotectonic activity on Olympus Mons, *J. Geophys. Res. Planets*, 112,
926 doi:10.1002/2016JE005108.
927 Peiterson, M.N., and D.A. Crown (1999), Downflow width behavior of Martian and terrestrial
928 lava flows, *J. Geophys. Res.*, 104, no. E4, 8473 – 8488.
929 Pieri, D.C., Baloga, S.M., Nelson, R.M., and C. Sagan (1984), Sulfur Flows of Ra Patera, IO,
930 *Icarus*, 60, 685 – 700.
931 Pinkerton, H. (1987), Factors affecting the morphology of lava flows, *Endeavour New Series*, 11,
932 no. 2, 73–79.
933 Pinkerton, H., and R.S. J. Sparks (1976), The 1975 Sub-terminal lavas, Mount Etna: A case
934 history of the formation of a compound lava field, *J. Volcanol. Geotherm. Res.*, 1, 167 – 182.
935 Pinkerton, H., James, M., and A. Jones (2002), Surface measurements of active lava flows on
936 Kilauea volcano, Hawai'i, *J. Volcanol. Geotherm. Res.*, 113, 159 – 176.
937 Plescia, J.B. (2004), Morphometric properties of Martian volcanoes, *J. Geophys. Res., 109,*
938 E03003, doi: 10.1029/2002JE002031.
939 Rogers, A.D., and P.R. Christensen (2007), Surface mineralogy of Martian low-albedo regions
940 from MGS-TES data: implications for upper crustal evolution and surface alteration, *J.*
941 *Geophys. Res.*, 112, E01003, doi: 10.1029/2006JE002727.
942 Rowland, S.K., Harris, A.J.L., and H. Garbeil (2004), Effects of Martian conditions on
943 numerically modeled, cooling-limited, channelized lava flows, *J. Geophys. Res.*, 109,
944 E10010, doi: 10.1029/2004JE002288.
945 Sakimoto, S.E.H., Crips, J., and S.M. Baloga (1997), Eruption constraints on tube-fed planetary
946 lava flows, *J. Geophys. Res.*, 102, no. E3, 6597 – 6613.

947 Sakimoto, S.E.H., and T.K.P. Gregg (2001), Channeled flow: analytic solutions, laboratory
948 experiments, and applications to lava flows, *J. Geophys. Res.*, 106, no. B5, 8629–8644.
949 Scott, D.H., and K. L. Tanaka (1981), Mars: Paleostratigraphic restoration of buried surfaces in
950 Tharsis Montes, *Icarus*, 45, 304 – 319.
951 Self, S., Thordarson T., Kesthelyi, L., Walker, G.P.L., Hon, K., Murphy, M.T., Long, P., and S.
952 Finnemore (1996), A new model for the emplacement of Colombia River basalts as large,
953 inflated pahoehoe lava flow fields, *Geophys. Res. Lett.*, 23, no. 19, 2689–2692.
954 Self, S., Thordarson, T., and L. Keszthelyi (1997), Emplacement of Continental Flood Basalt
955 Lava Flows, *Geophys. Monograph.*, 100, 381 – 410.
956 Self, S., Jay, A.E., Widdowson, M., and L.P. Keszthelyi (2008), Correlation of the Deccan and
957 Rajahmundry Trap lavas: Are these the longest and largest lava flows on Earth?, *J. Volcanol.*
958 *Geotherm. Res.*, 172, 3 – 19.
959 Sheth, H.C., 2006. The emplacement of pahoehoe lavas on Kilauea and in the Deccan Traps. *J.*
960 *Earth Systems Sci.*, 115, 615–629.Soule, S.A., and K.V. Cashman (2004), The mechanical
961 properties of solidified polyethylene glycol 600, an analog for lava crust, *J. Volcanol.*
962 *Geotherm. Res.*, 129, 139–153.
963 Spudis, P.D., McGovern, P.J., and W.S. Kiefer (2013), Large shield volcanoes on the Moon, *J.*
964 *Geophys. Res. Planets*, 118, 1063 – 1081, doi: 10.1002/jgre.20059.
965 Vicari, A., Alexis, H., Del Negro, C., Coltelli, M., Marsella, M., and C. Proietti (2007),
966 Modelling of the 2001 lava flow at Etna volcano by cellular automata approach,
967 *Environment. Model. Software*, 22, 1465–1471.
968 Wadge, G. (1981), The variation of magma discharge during basaltic eruptions, *J. Volcanol.*
969 *Geotherm. Res.*, 11, 139–168.

970 Walker, G.P.L. (1971), Compound and simple lava flows and flood basalts, *Bull. Volcanol.*, 35,
971 579 – 590.

972 Walker, G.P.L. (1973), Lengths of lava flows, *Phil. Trans. R. Soc. Lond. A.*, 274, 107 – 118.

973 Werner, S.C. (2009), The global martian volcanic evolutionary history, *Icarus*, 201, 44 – 68.

974 Wilson, L., J.W. Head III (1983) A comparison of volcanic eruption processes on Earth, Moon,
975 Mars, Io, and Venus, *Nature*, 302, 663 – 669.

976 Wolfe, E.W., Garcia, M.O., Jackson, D.B., Koyanagi, R.Y., Neal, C.A., and A.T. Okamura
977 (1987), The Pu'u O'o eruption of Kilauea volcano, episodes 1 – 20, January 3, 1983, to June
978 8, 1984, 471 – 508.

979 Xiao, L., Huang, J., Christensen, P.R., Greeley, R., Williams, D.A., Zhao J., and Q. He (2012),
980 Ancient volcanism and its implication for thermal evolution of Mars, *Earth and Planet. Sci.*
981 *Lett.*, 323-324, 9 – 18.

982 Zuber, M.T., D.E. Smith, S.C. Solomon, D.O. Muhleman, J.W. Head, J.B. Garvin, J.B. Abshire,
983 and J.L. Bufton (1992), The Mars observer laser altimeter investigation, *J. Geophys. Res.*, *97*,
984 7781 – 7797.